Air Force Institute of Technology

AFIT Scholar

3-2005

Optical Investigation of Transition Metal Implanted Wide Band Gap Semiconductors

Brian P. Feller

Follow this and additional works at: https://scholar.afit.edu/etd

Part of the Atomic, Molecular and Optical Physics Commons

www.manaraa.com

OPTICAL INVESTIGATION OF TRANSITION METAL IMPLANTED

WIDE BAND GAP SEMICONDUCTORS

THESIS

Brian P. Feller, First Lieutenant, USAF

AFIT/GEO/ENP/05-02

DEPARTMENT OF THE AIR FORCE
AIR UNIVERSITY
AIR FORCE INSTITUTE OF TECHNOLOGY

Wright-Patterson Air Force Base, Ohio

APPROVED FOR PUBLIC RELEASE; DISTRIBUTION UNLIMITED

The views expressed in this thesis are those of the author and do not reflect the official policy or position of the United States Air Force, Department of Defense, or the United States Government.

AFIT/GEO/ENP/05-02

OPTICAL INVESTIGATION OF TRANSITION METAL IMPLANTED

WIDE BAND GAP SEMICONDUCTORS

THESIS

Presented to the Faculty

Graduate School of Engineering and Management

Air Force Institute of Technology

Air University

Air Education and Training Command

in Partial Fulfillment of the Requirements for the

Degree of Master of Science in Electrical Engineering

Brian P. Feller, B.S.E.E.

First Lieutenant, USAF

March 2005

APPROVED FOR PUBLIC RELEASE; DISTRIBUTION UNLIMITED

AFIT/GEO/ENP/05-02

OPTICAL INVESTIGATION OF TRANSITION METAL IMPLANTED

WIDE BAND GAP SEMICONDUCTORS

Brian P. Feller, B.S.E.E.
First Lieutenant, USAF

Approved:

/SIGNED/	
Yung Kee Yeo (Chairman)	date

/SIGNED/	
Michael A. Marciniak (Member)	date

/SIGNED/	
James A. Fellows (Member)	date

Abstract

Thin films of GaN, $Al_{0.1}Ga_{0.9}N$, and ZnO were ion implanted with chromium (Cr), manganese (Mn), and nickel (Ni) at 200 keV to produce dilute magnetic semiconductor materials. Optical and magnetic techniques were used to evaluate crystal structure restoration and coercive field strength as a function of implant species and annealing temperature. The results of cathodoluminescence measurements showed that near band edge transitions dominant in as-grown samples were dominated by other emissions after implantation. The near band edge transitions returned to prominence in the properly annealed samples, and were reduced in prominence for over-annealed samples. Magnetic impurity related emissions were observed in $Al_{0.1}Ga_{0.9}N$ for Cr (3.3 eV) and Mn (3.25 eV), and in ZnO for Ni (2.55 eV). Maximum crystal restoration was obtained for $Al_{0.1}Ga_{0.9}N$ implanted with Cr, Mn, or Ni after annealing at 675 ^{o}C for 5 minutes; for the p-GaN implanted with Cr after annealing at 750 ^{o}C for 5 minutes; for the p-GaN implanted with Mn or Ni after annealing at 675 ^{o}C for 5 minutes; for the ZnO implanted with Cr after annealing at 700 ^{o}C for 10 minutes; for the ZnO implanted with Mn after annealing at 675 ^{o}C for 10 minutes; and for the ZnO implanted with Ni after annealing at 650 ^{o}C for 10 minutes. Maximum coercive field strengths were found for the $Al_{0.1}Ga_{0.9}N$ implanted with Cr after annealing at 750 ^{o}C for 5 minutes; for the $Al_{0.1}Ga_{0.9}N$ implanted with Mn after annealing at 675 ^{o}C for 5 minutes; for the $Al_{0.1}Ga_{0.9}N$ implanted with Ni after annealing at 700 ^{o}C for 5 minutes; for the p-GaN implanted with Cr or Mn after annealing at 725 ^{o}C for 5 minutes; for the p-GaN

implanted with Ni after annealing at 675 ^{o}C for 5 minutes; for the ZnO implanted with Cr

or Ni after annealing at 725 ^{o}C for 10 minutes; and for the ZnO implanted with Mn after

annealing at 725 ^{o}C for 10 minutes. In general, the optimum annealing conditions for

best optical and magnetic properties of the implanted wide band gap semiconductors

agree with each other very well.

Acknowledgments

I would like to express my appreciation to Dr Yung Kee Yeo for his guidance throughout this project and his continued support of my academic career. I would also like to thank Jeremy Raley for the equipment training, advice, and data access that made the link between our two projects possible. Finally I would like to thank Dr Michael Marciniak and Lt Col Jim Fellows for their consideration in serving as committee members for this project.

Brian Feller

Table of Contents

List of Figures

List of Tables

OPTICAL INVESTIGATION OF TRANSITION METAL IMPLANTED
WIDE BAND GAP SEMICONDUCTORS

I. INTRODUCTION

Wide band gap semiconductors such as GaN, AlGaN, and ZnO are a major area of interest in the fields of physics and electrical engineering for their suitability to a wide variety of device applications. One aspect of these materials which is important to the Department of Defense, particularly the Air Force, is the inherent resistance to radiation effects found in wide band gap semiconductor materials. Research in this area will mature wide band gap semiconductor materials science, enabling the construction of electronic devices from these materials. Making devices from these substances eliminates a vulnerability found in standard electronic systems, which reduces the need to shield against radiation threats or hostile environments such as high temperatures or cosmic radiation found in space.

Since the bulk of the development of electronics has centered on traditional semiconductor materials such as silicon and gallium-arsenide, methods for producing electronic devices using these materials are well understood. Years of research have gone into refining doping and annealing processes for use with these materials. Adjusting manufacturing processes to use wide band gap semiconductors requires that we repeat much of this basic research.

Also of major interest to the military, is the evolution of spin transport electronics (spintronics). This research could support the development of a new class of spintronic

1

devices and circuits, including spin transistors, optical emitters with polarized output, magnetic sensors, magnetic random access memories, and quantum computing devices.

While much work has been published recently concerning wide band gap semiconductors, there remain several areas of this basic research that have not been well studied to date. This thesis will fill in some of these areas, specifically, it will address annealing temperatures and their effects on magnetic properties of transition metal implanted p-GaN, $Al_{0.1}Ga_{0.9}N$, and ZnO. The transition metals being discussed are chromium, nickel, and manganese.

Project Overview

This project was carried out as underlying research in support of an ongoing dilute magnetic semiconductor research project being conducted by Capt Jeremy Raley to investigate high-temperature ferromagnetism in transition metal implanted wide band gap semiconductors. A successful combination of annealing times and temperatures should maximize both crystal recovery and activation of ferromagnetic dopants in the resultant crystal.

The focus of this work was to develop guidelines for annealing these materials with respect to both the recovery of the basic crystalline behavior of the semiconductors and the activation of ferromagnetic elements within them. Secondary objectives included evaluating the potential of these material combinations, and reporting the research results including any previously unpublished properties discovered.

Optical investigation of variously annealed samples was accomplished by taking cathodoluminescence spectra. Data analysis for this project was based on these

2

measurements and magnetic hysteresis measurements, previously accomplished by Jeremy Raley using a superconducting quantum interference device (SQuID).

The following chapters will describe this project in detail, starting with an overview of some basic principles helpful in understanding the work. Next, it will describe, in detail, the experimental procedures used in performing this research, including a discussion of the data analysis process. The results will then be presented and discussed, including observed patterns in the data, ties between the optical and magnetic results, and an outline of areas of potential future work.

II. THEORY

The following chapter outlines some theoretical principles useful in understanding the goals and methods of this project. It addresses wide band gap semiconductors in general and the importance of crystal structure, including common processes used in fabricating devices. This is followed by a brief introduction to important concepts in both optical and magnetic properties.

Wide Band Gap Semiconductors

A semiconductor exhibits a certain range of the absence of allowed electronic energy states at room temperature. Semiconductors commonly used in microelectronics have a band gap of around 1 electron Volt (eV). A general introduction to basic solid state physics and energy band behavior appears in Chapters 1 and 9 in McKelvey's Solid State Physics. [1]

What are wide band gap semiconductors?

Materials with a larger gap in allowed energy states (between 2.5 and 4 eV) were formerly classed as insulators. Increasing constraints on the allowable behavior and necessary properties of semiconductor electronics have sparked research into using different materials. Recently the line between semiconductor and insulator has been pushed to about 4 eV to allow the class of wide band gap semiconductors. These materials offer several innate advantages over classical semiconductors for many applications. Thermal excitation of carriers has become a major concern in modern electronics, because as the thermal carriers begin to dominate the system, intentionally implanted areas of the semiconductor change their behavior. [2:522-524]

4

Why are they important?

The most significant and pervasive problem with modern electronics is their vulnerability to excessive heat. For many years the limiting factor of computer processor speed was the ability of the system to dissipate heat quickly enough for long term operation at higher switching speeds. Each major improvement in technology or architecture that allowed less heat build-up in a computer chip has led directly to the next generation of faster processors.

The mechanism causing a semiconductor to malfunction with overheating is thermal generation of carriers. As temperature increases, more and more electrons can achieve enough energy to cross the band gap and become extraneous charge carriers. Smaller feature sizes and lower operating currents were two improvements in electronic circuits that reduced thermal generation. These effects had a drawback however, in that while they reduced the magnitude of heat build up in a device, they also reduced the tolerance to leakage currents caused by extraneous carriers. At sufficiently high temperatures, the thermally generated carriers will completely dominate any practical doping level of intentional carriers.[2:43] This places strict limits on the operating temperature of any electronic device. Using materials with a wider band gap dramatically reduces the generation of thermally excited carriers, increasing the heat tolerance of the device.

Other mechanisms also increase unintentional carriers in a device. Incident radiation from any source can also generate ions and trapped charges and can cause device failure. Increasing the band gap reduces the effects of these problems as well.

Wide band gap semiconductors also offer a broader range of physical characteristics than traditional semiconductor materials. They are generally stronger,

5

harder to damage physically, and have higher melting points than classical semiconductors like silicon and gallium arsenide. Wide band gap materials are usually transparent to visible light which provides significant advantages for applications such as solar blind radiation detectors. Some of these materials offer highly controllable electrical properties. Gallium nitride can exhibit room temperature resistivities from 18 to 450 Ω-cm depending on doping level. [3]   Certain materials such as zinc oxide also allow significantly higher thermal conductivity at lower electrical conductivity than other semiconductor materials.[4]

Crystal Structure

As in any semiconductor, the uniform arrangement of atoms is the foundation for the predictable behavior of the material. This, in turn, is essential for engineering devices to take advantage of the material. In order to use new materials in electronic devices, it will be necessary to alter the composition of the material, without irreparably damaging the crystal structure. In short, most of the damage done in implanting new atoms must be repaired.

Ion Implantation

The most easily controlled method for introducing dopant atoms into a semiconductor material is by ion implantation. Charged atoms of the dopant species are ionized and electrically accelerated into the crystal substrate. By varying the dose and implantation energy, this method can be used to produce virtually any desired doping profile. This method is relatively inexpensive and easily patterned, but causes significant damage to the crystal structure of the substrate. It is the most commonly used doping method for bulk crystal materials.[2:469-480]

6

Annealing

In order to repair the damage caused by ion implantation, and/or to activate the dopant atoms causing them to behave as a part of the crystal, an implanted crystal substrate is usually annealed at a high temperature. This process holds an increased level of vibrational energy within the crystal making it easier for atoms to break and form inter-atomic bonds, allowing natural inter-atomic interaction to shift the atoms back into a more regular physical arrangement.

Time and temperature are the variable parameters of an annealing operation. If a material is insufficiently annealed by using either too low a temperature, or an insufficient time, the damage to the crystal will not be repaired. If a crystal is annealed at too high a temperature or for too long, additional damage may occur.[2:469-480]

Proper times and temperatures for annealing are generally determined experimentally and refined for each specific substrate, dopant, and manufacturing process. A major aim of this project is to determine annealing conditions for AlGaN, GaN, and ZnO doped with Cr, Mn, and Ni, that can be used as starting points for future experiments. A proper anneal will activate the dopants, and recover the general crystal properties of the as-grown crystal.

Optical Properties

The quality of a semiconductor crystal can be measured by looking at the light output from the crystal when it is excited by an energy source. This is called luminescence of the material. There are many features present in emission spectra that are not discussed here and do not affect the work in this project. For a more

www.manaraa.com

comprehensive description of luminescence spectral features, see Bhattacharya's
Semiconductor Optoelectronic Devices, Chapter 3. [5:113-154]

Light emission in crystals

As electrons in a semiconductor relax from an excited state, energy is released
equal to the difference between the energy levels of the excited state and the ground state.
In a direct band gap material, the transition from the lowest energy states in the
conduction band to the highest energy states in the valence band involves a large change
in energy with minimal change in momentum. This results in the generation of a photon.
Statistically significant repeated transitions releasing photons of similar energy can be
observed as light emission from the crystal surface, and results in a peak of light emission
at a wavelength corresponding to that energy.[5:113-154]

Band Edge Feature

Good quality crystals exhibit emissions which are of predictable energies. In
undoped crystals of good quality, the vast majority of excited electrons will leave
vacancies that relax to the top of the valence band. These excited electrons generally
relax through very fast non-radiative processes until they occupy energy states near the
bottom of the conduction band just prior to radiative transition back to lower energy
states near the top of the valence band.

Because the arrangement of atoms in a perfect crystal is uniform, a good quality
undoped semiconductor crystal can emit photons with energies at or just below the band
gap. Although in a perfect crystal, there are no allowed states within the gap, the
electrons can transition radiatively to the vacancies in the valence band through excitonic
emission with photon energies slightly below the band gap. A real crystal will inevitably
contain unintentional dopants or defects usually resulting in shallow energy states within

8

the band gap. Thus the luminescence spectra of good quality undoped direct band gap crystals show dominant peaks very near band gap energies with no significant emission at other energies.[5:113-154] These are called the band edge feature of the emission spectrum, and are the most significant feature present in as-grown material luminescence measurements.

Impurity Emission Peaks

A desirable feature of the emission spectrum in a implanted crystal is the presence of a peak within the band gap that corresponds to the dopant species interacting with the crystal itself.[5:113-154] This will be an emission peak that is not present in the as grown material. This peak must also not correspond to the energy of atomic transitions in the dopant species, because that would indicate luminescence from excited electrons of just the dopant atoms, and would not support the conclusion that the dopants are interacting with the crystal. The location of these peaks may be important indicators of the electrical and optical behavior of the implanted crystal.

Dislocation/Vacancy Emission

Imperfections in the crystals result in emission at different energies than the band gap of the material or the impurity emission peak. A well documented broad band emission called the *yellow band* occurs in GaN near 2.1 to 2.3 eV, which has been attributed to dislocations and other defects in the lattice structure.[6] A similar band called the *green band* appears in ZnO around 2.3 to 2.5 eV.[7:643-646] These emission bands are indicators of poor crystal recovery, and generally dominate as-implanted emission spectra. These features will be reduced, in properly annealed crystals.

9

Crystal Recovery

A combination of the first two previously discussed features is used to benchmark the crystal recovery of the crystal following ion implantation and subsequent annealing. The dominance of either the band edge emission or an impurity peak over other emission sources will indicate a well-recovered crystal.

Magnetic Activation

Just like any dopant introduced into a semiconductor crystal, the transition metals used in this project need to become part of the crystal and have their arrangement fixed within the crystal to behave predictably. The main difference with these materials is that the desired interaction is not purely opto-electrical in nature. It is possible that the best magnetic results for a material combination may be obtained with the impurities trapped interstitially within the crystal, instead of being incorporated into a lattice site. If this is the case, the best hysteresis result will require different (probably lower temperature) annealing conditions than the best optical response. In either case, it will generally be necessary for a material to undergo some kind of annealing process before the magnetic properties become active in the semiconductor.

Hysteresis

Hysteresis is the ability of a material to store a magnetically induced field. This is the primary measure of the magnetic activation that is the focus of the overarching dissertation project. Hysteresis is measured by alternately applying a strong positive and negative magnetic field and measuring the magnetic field at the sample. A material exhibits a strong hysteresis effect if it holds a magnetic field with zero applied field after exposure. Figure 1 is an example of a hysteresis measurement result showing.
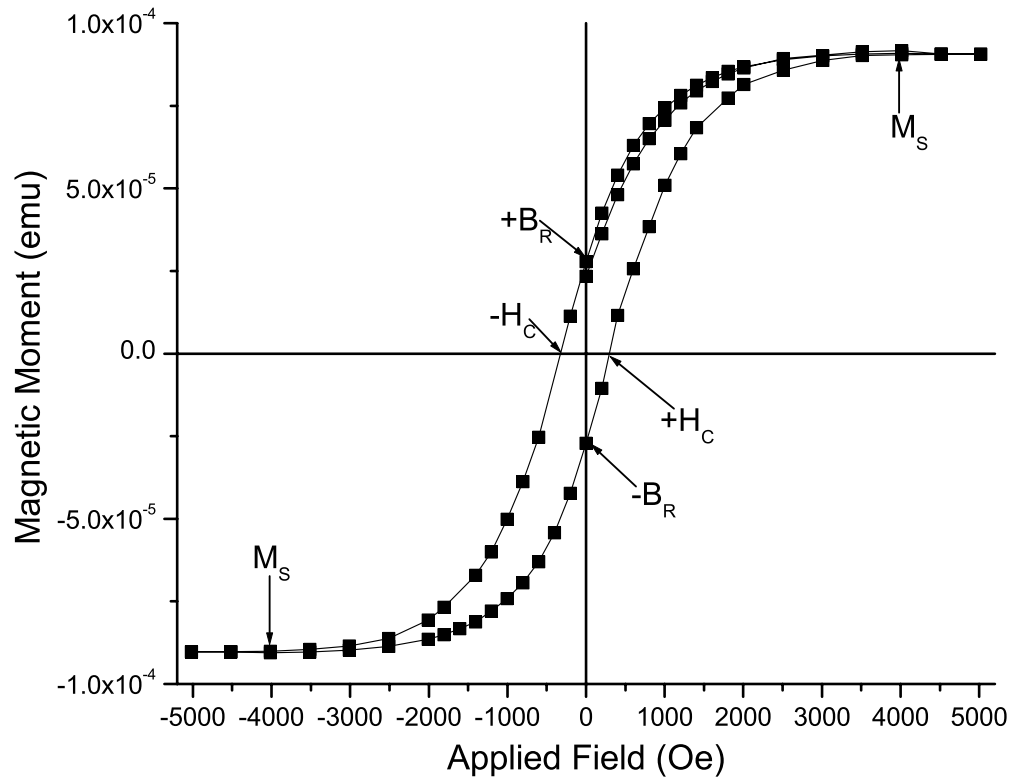
10

Figure 1. Hysteresis measurement example. This diagram is a graphical
representation of magnetism versus applied field, showing a magnetic
hysteresis loop with coercive (H_C) and remnant (B_R) fields and saturation
magnetization (M_S) labeled.

Annealing effects on Hysteresis

Annealing has a strong effect on the strength of a field induced by a reference
field. The strength of the hysteresis effect thus may sometimes be used as another
indicator of crystal structure recovery. It is also possible that interstitial impurities may
have a strong hysteresis effect. In this case, enough annealing to heal some of the crystal
damage and trap the impurity atoms in place without being enough to incorporate the
dopant into a crystal lattice site may provide the maximum measurable hysteresis.

11

Graphs showing preliminary measurements from Jeremy Raley's work appear in the Appendix.

Summary

This chapter has introduced concepts important to understanding the work done in this project. The following chapter contains detailed descriptions of the procedures used in each stage of the project.

III. Experiment

This chapter details the procedures used throughout this project, from obtaining and preparing materials for testing, through testing procedures and equipment. It includes a discussion of the data analysis process and leads the reader through this process for one material combination.

Crystal Growth

Crystal samples were obtained from sources outside AFIT. A sapphire wafer with a 2 μm thick aluminum nitride (AlN) buffer layer, and a 1 μm thick epitaxial layer of p-type gallium nitride (p-GaN) grown with 10^{17} Mg atoms/cm^3 was ordered from Epiplus. Another sapphire wafer with a 2 μm thick buffer layer of AlN and a 1 μm thick epitaxial layer of 10% mole fraction aluminum gallium nitride ($Al_{0.1}Ga_{0.9}N$) was ordered from SVT associates. A sapphire wafer with a 1 μm thick epitaxial layer of zinc oxide (ZnO) was grown by Rutgers University. One wafer of each material was obtained, and diced into quarters which were used for different dopants. Since one wafer is used for all testing of each material, various samples can be compared directly, minimizing errors due to variations in growth processes.

Ion Implantation

Three sections of each wafer were sent to Implant Sciences for ion implantation, with the fourth section of each saved as an as-grown control sample. One section of each material was implanted with 5 x 10^{16} Cr atoms/cm^2. A second section of each material was implanted with 5 x 10^{16} Mn atoms/cm^2. The third section of each material was implanted with 3 x 10^{16} Ni atoms/cm^2. Implantation energy of 200 keV was used for

13

each implantation. The sections were then returned to AFIT where they were diced into samples approximately 5 by 5 mm.

Annealing

Holding some samples of each material with each dopant for as-implanted measurements, samples were annealed for various times and temperatures. All annealing operations were conducted using a small quartz tube furnace with actual furnace temperatures recorded every 15 seconds to maintain a history of the heating profile. There was relatively minor variation in time versus temperature profiles of the furnace indicating that variability in the annealing process is unlikely to be a source for error in this study.

Annealing of ZnO was conducted in an oxygen rich environment, provided by flowing oxygen gas through the furnace tube throughout the annealing operation. Annealing of p-GaN and $Al_{0.1}Ga_{0.9}N$ were conducted in a nitrogen rich environment by flowing 99.999% pure gaseous nitrogen through the furnace. The gas rich environments were established to minimize out-gassing of the oxygen or nitrogen from the respective crystals.

Superconducting Quantum Interference Device (SQuID) Measurement

SQuID measurements analyzed for this project were taken from preliminary results obtained by Jeremy Raley. This project used the single number reported for coercive field strength as a sole measure of magnetic effectiveness of the material for each annealing case.

14

Cathodoluminescence Measurement

Cathodoluminescence (CL) is the process of exciting a material by adding energy in the form of a beam of accelerated electrons, causing the subsequent release of photons as electrons in the substance relax to their less energetic states. A schematic diagram of the equipment configuration used for these measurements appears in Figure 2.

For this study, CL was excited by a 10 keV electron beam at approximately 50 μA current provided by a Kimball Physics EMG-12 Electron Gun and EGPS-12 power supply. The path between the beam source and the target, as well as the environment of the target, was held at a vacuum pressure of approximately 7×10^{-8} Torr. The substrates were held at around 6 Kelvin using a cold head and a closed cycle helium compressor driven by a Lakeshore 330 Temperature Controller.

Spectra were taken using a Spex 0.5 m monochromator and a liquid-nitrogen cooled (to -35 ^{o}C) GaAs Photomultiplier tube at 1500 V, connected to a personal computer (PC) to record the output and control the selected wavelengths of the monochromator. The path between the target and monochromator is air with a glass door and two lenses to collimate and refocus the emitted light. Extraneous light appears near 700 nm in all measurements. This noise is inherent in the system, and is believed to be due to warming of the cathode in the electron gun. This limits the useable frequency range to below 680 nm.
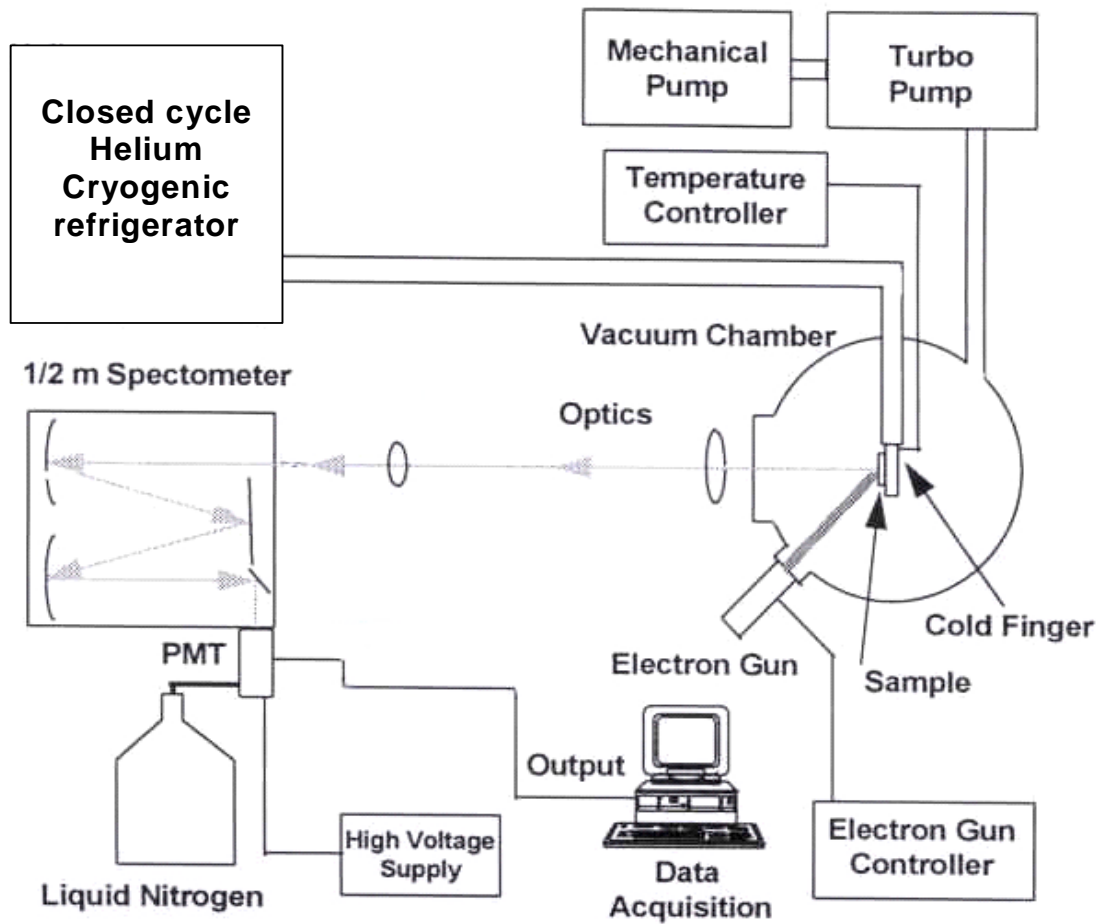
15

Figure . Schematic diagram of a cathodoluminescence system used to collect
spectra.[8]

Repeated measurements were taken for each case presented as the best anneal for

a material/dopant combination. Measurements were also repeated for cases

demonstrating anomalous results.

Sample Storage and Treatment

Samples used in this study were stored in protective envelopes, in a humidity-

controlled environment (low humidity clean room or a plastic container, stored with

moisture absorbing silica crystals). They were handled with tweezers, marked for

16

identification purposes on the back side with a diamond scribe, and cleaned with acetone as necessary.

Analyzing Data

The primary data to be analyzed in this study was the luminescence spectra from the CL measurements. Emission spectra were recorded for a range of annealing temperatures and visually inspected for the prominence of desirable features, and the reduction of undesirable emissions. Ideally, a range of temperatures was tested for each material combination covering a discernable progression from lower temperature anneals, through the annealing condition giving the best results, to higher temperature anneals showing additional damage. This validates the designation of a good annealing recipe by demonstrating that there is no improvement made going to either extreme in temperature.

The following is an example outlining the process of analyzing a set of these spectra. All spectra discussed in this example are graphed showing relative intensity, such that the highest feature on each spectrum reaches the approximate top of the graph.

Figure 3 shows a typical measurement for as-grown $Al_{0.1}Ga_{0.9}N$. The only significant feature of this spectrum is the prominent band edge feature. This was used as an example to compare annealed cases against. In Figure 4, the same material is shown after implantation. The primary features in this graph are emissions due to undesirable sources such as crystal damage, and indicate ranges of emission that a good annealing recipe will reduce. More importantly, the band-edge feature, which will be recovered with a good anneal, is not present in this measurement.
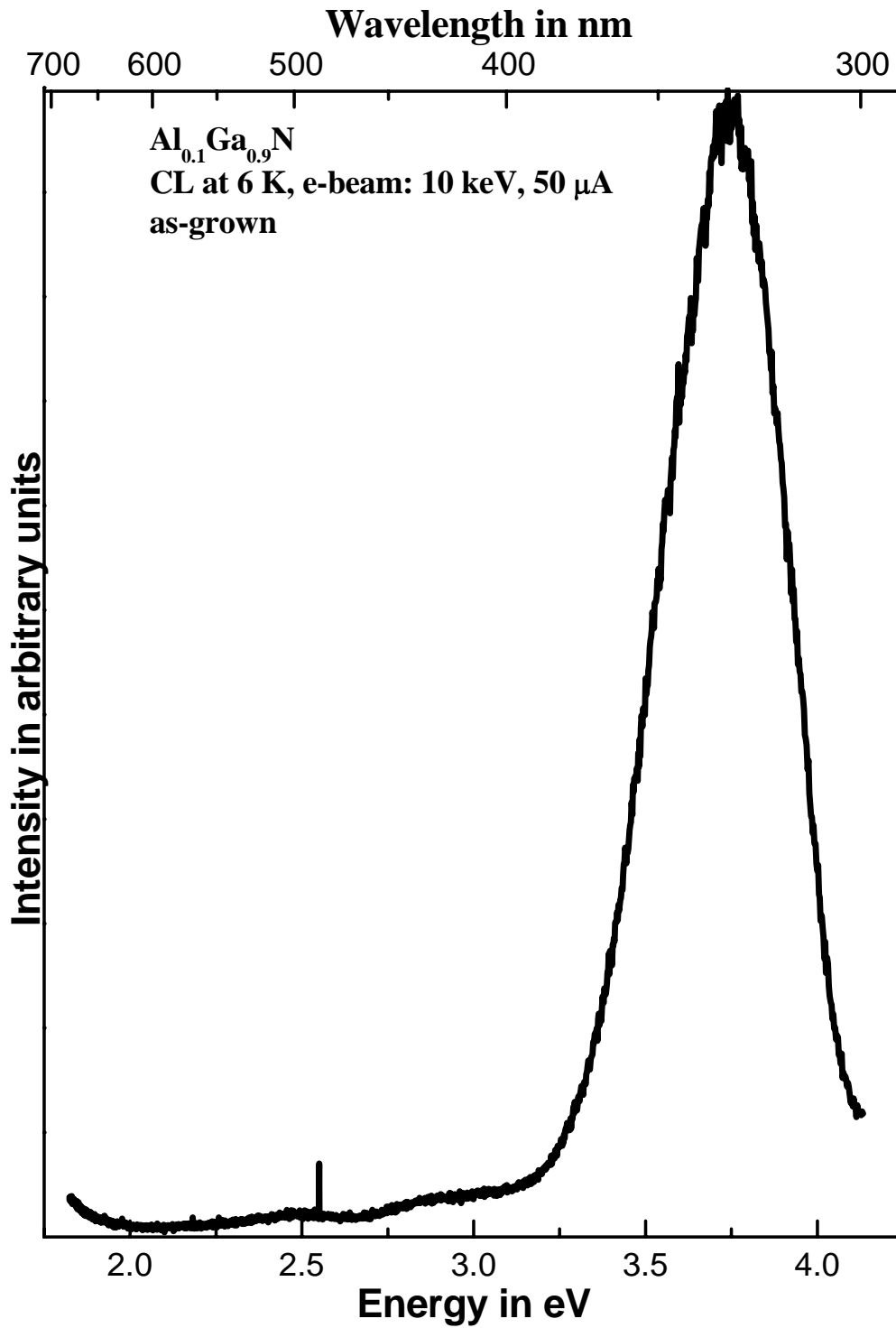
17

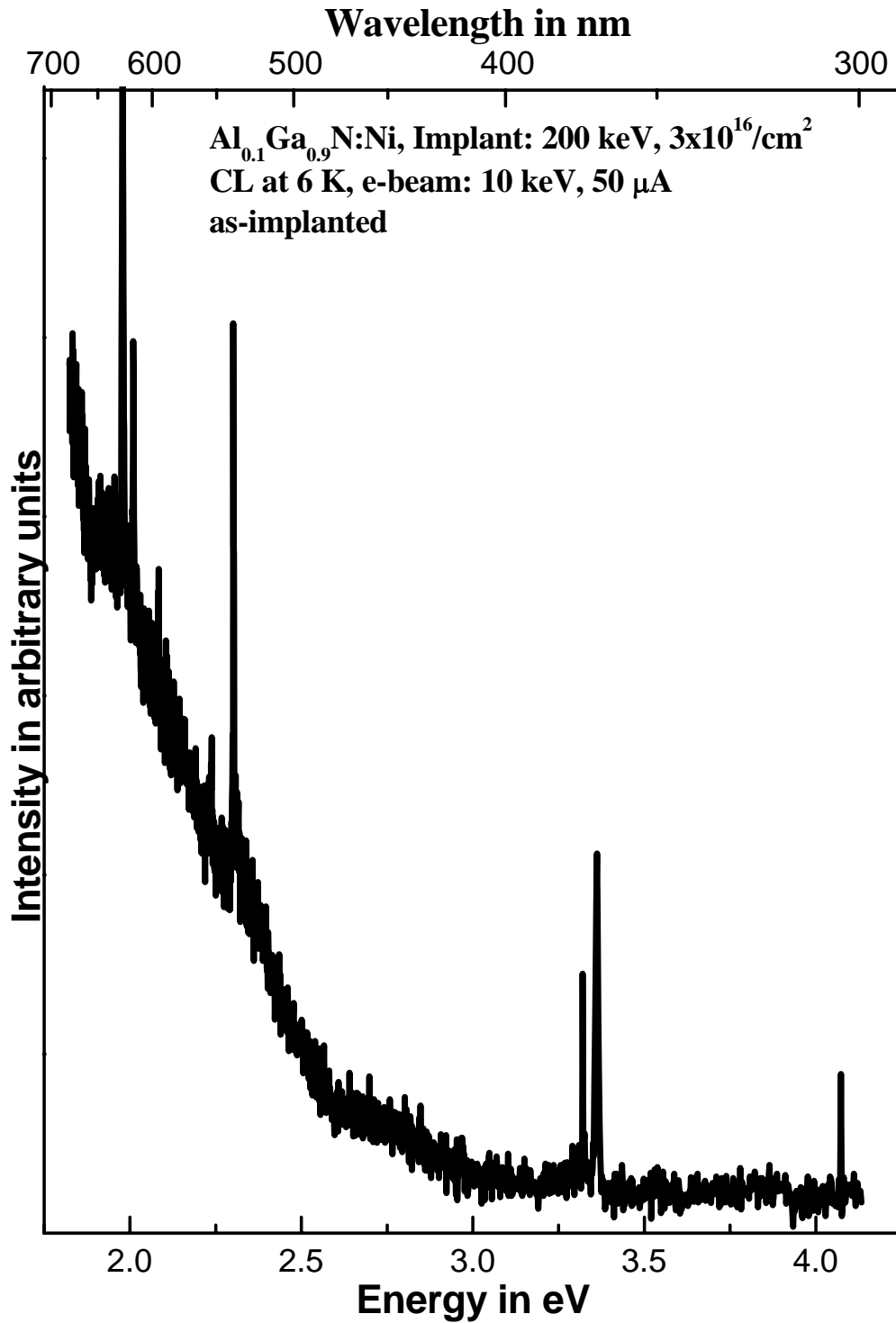Figure 3. Cathodoluminescence spectrum of as-grown $Al_{0.1}Ga_{0.9}N$.

Figure 4. Cathodoluminescence spectrum of $Al_{0.1}Ga_{0.9}N$ implanted with nickel. Figure 5 is an under-annealed case. Some improvement can be seen in the

presence of a relatively small feature near the band edge, but the spectrum remains

19

dominated by emission in the ranges shown in the as-implanted measurement. The best anneal found for this particular material is shown in Figure 6. The band edge is once again prominent in the spectrum, and while it is not shown in this example, there may be new features noticeable at this point that can be attributed to the dopant species interacting with the crystal structure. Figure 7 shows an over-annealed case in which the areas of the spectrum shown to be due to poor crystal properties are once again dominating emission from the sample.

If an impurity peak is noticed in the well-annealed cases for a material, it must be checked against other potential causes of the emission to increase confidence that it is due to proper interaction between the dopant and the crystal. One important source to check is the simple atomic emission of the dopant species. Since care is taken to ensure that other atoms are not introduced into these samples and most other possible emission sources would show up in as-grown measurements, it is reasonable to conclude that any peaks would be due in some way to the dopant atoms. Table 1 shows the known atomic spectral lines of the dopant species used in this study.

Table 1. Atomic Emission Lines of Transition Metal Species. (**Bold** entries denote strong emission lines.) [9]

Chromium		manganese		nickel	
Wavelength(nm)	Energy(eV)	Wavelength(nm)	Energy(eV)	Wavelength(nm)	Energy(eV)
425.435	**2.914**	**403.076**	**3.076**	**341.476**	**3.631**
357.869	3.465	257.610	4.813	**352.454**	**3.518**
359.349	3.450	279.482	4.436	232.003	5.344
360.533	3.439	279.827	4.431	349.296	3.550
427.480	2.900	403.307	3.074	351.505	5.527
428.972	2.890	403.449	3.073	361.939	3.426
520.844	2.380				

Figure 5. Cathodoluminescence spectrum of $Al_{0.1}Ga_{0.9}N$ implanted with nickel and annealed for 5 minutes at 650 $^{\circ}$C.
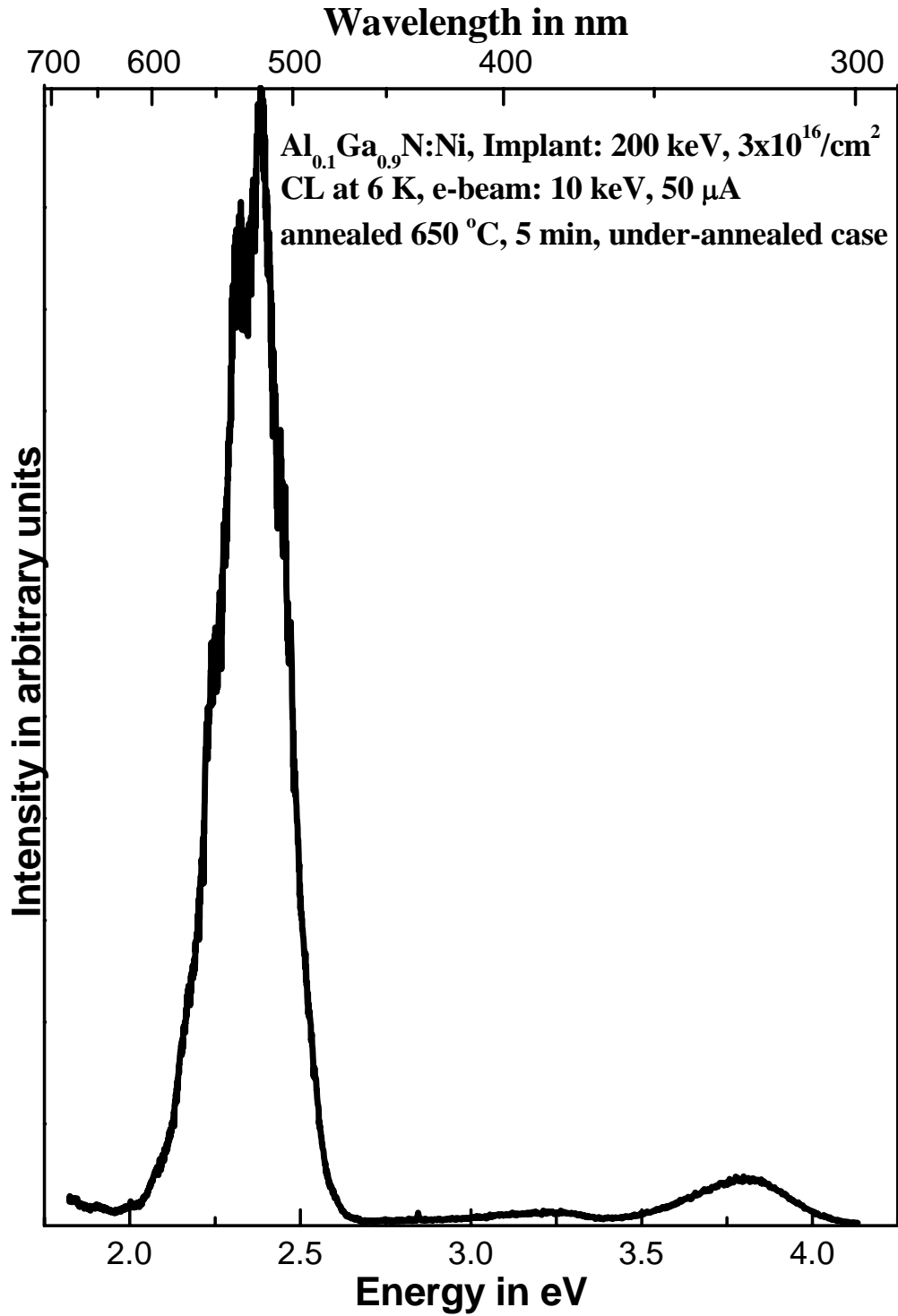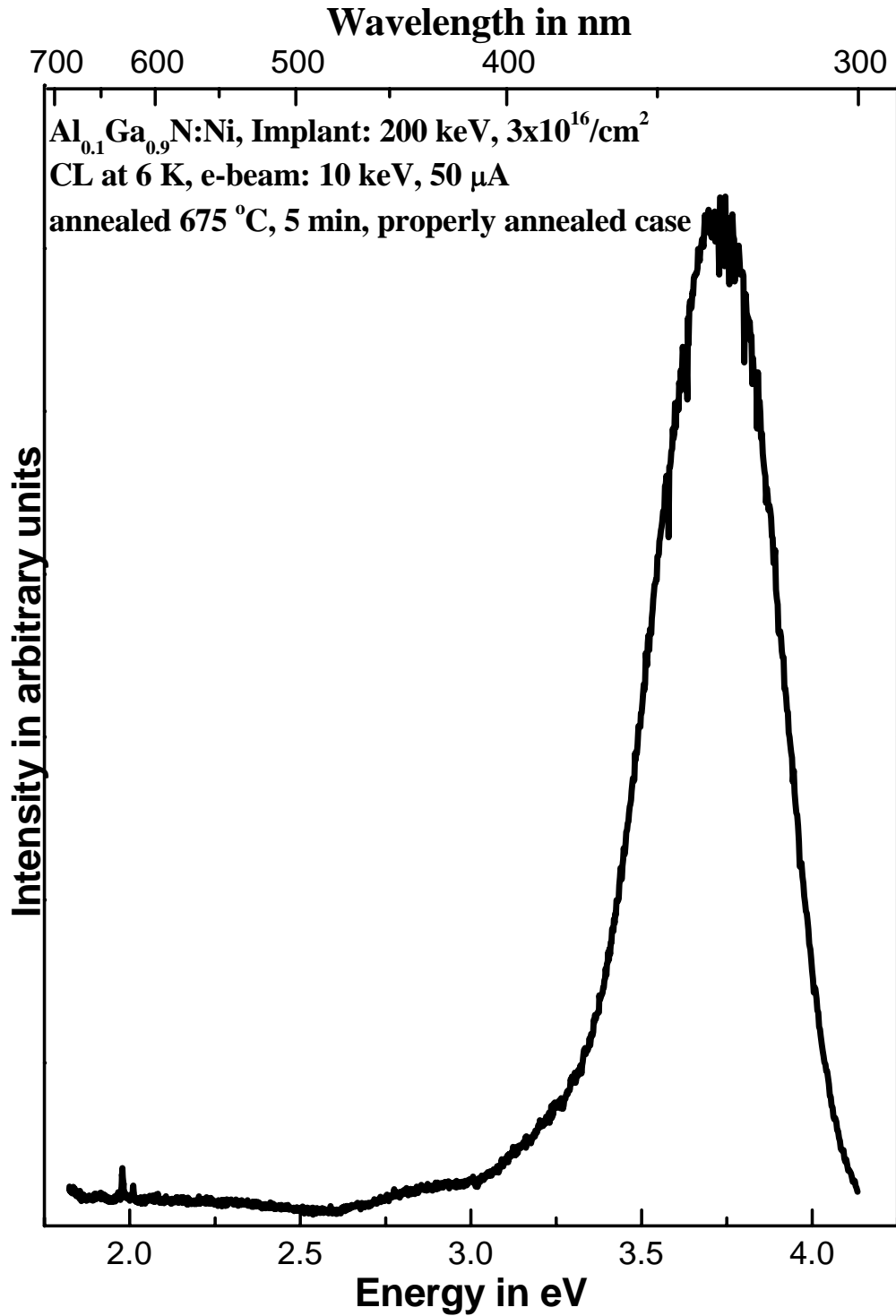
21

Figure 6. Cathodoluminescence spectrum of $Al_{0.1}Ga_{0.9}N$ implanted with nickel and annealed for 5 minutes at 675 ^{o}C.
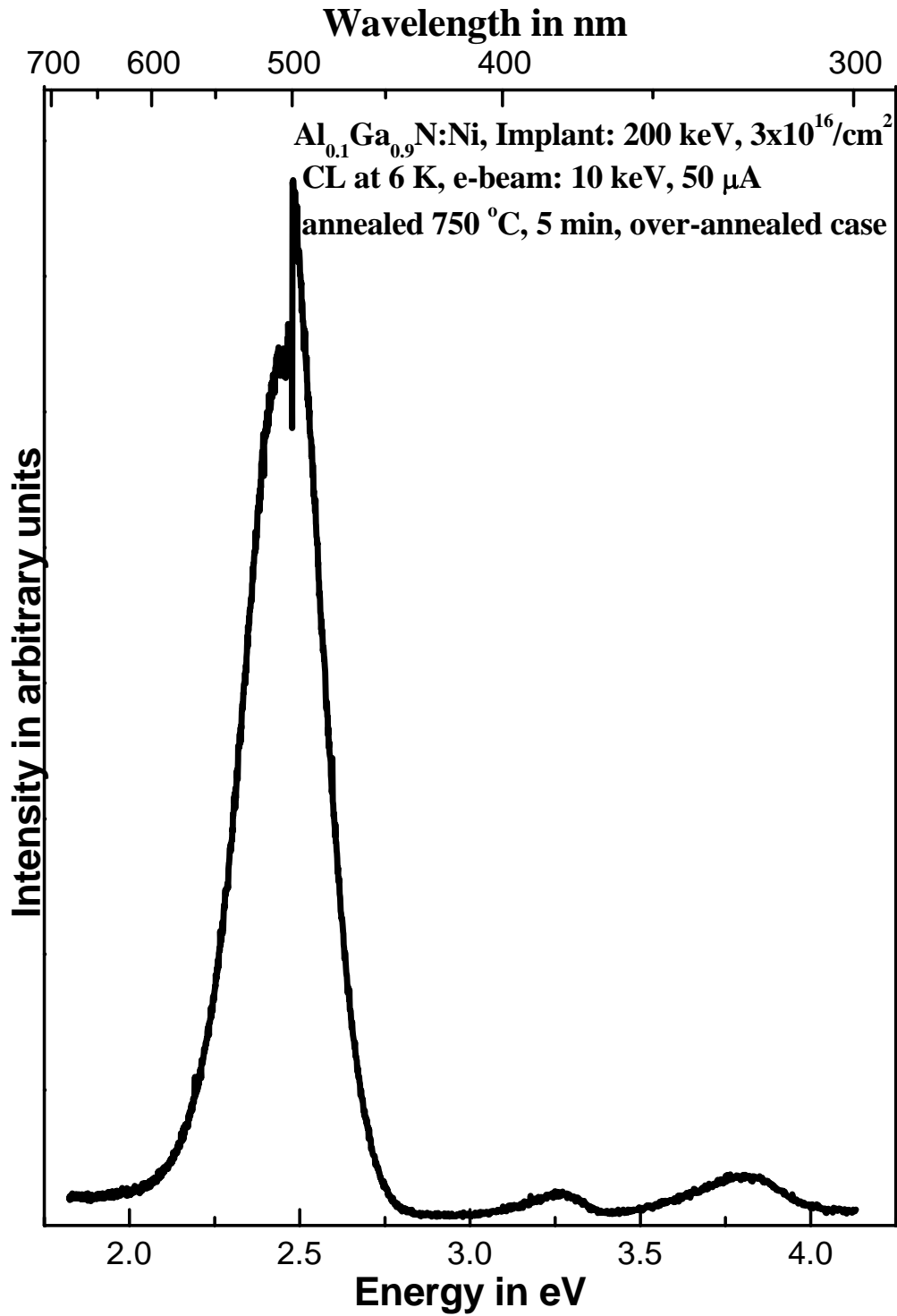
Figure 7. Cathodoluminescence spectrum of $Al_{0.1}Ga_{0.9}N$ implanted with nickel and annealed for 5 minutes at 750 ^{o}C.

The other piece of information analyzed for this study was the coercive field strength exhibited by the samples after each anneal. The same pattern was seen in these results as with the emission spectra. To ensure that the best anneal was obtained, a coercive field strength was sought which was higher than values for both lower and higher temperature anneals.

Summary

This chapter has detailed the procedures and equipment used in this project, both in processing samples, and taking measurements. It has also outlined the process by which data is analyzed and determinations are made of anneal quality. The following chapter will present and discuss the measurement results.

IV. Results and Discussion

This chapter presents the data obtained in this project. Graphs are displayed in a more standard format showing multiple spectra for the same material on each graph. The data is interpreted for each case, presenting the best result both optically and magnetically for each material/dopant combination.

$Al_{0.1}Ga_{0.9}N$

Figure 8 shows CL spectra for a $Al_{0.1}Ga_{0.9}N$ as-grown, as-implanted with Cr, and annealed at various temperatures. As can be seen in the graph, the optically determined best anneal was 675 ^{o}C for 5 min. The quality of the spectrum drops off at higher anneal temperatures. The band edge feature near 3.75 eV is prominent in the as grown and best anneal cases. The yellow luminescence common to GaN based materials is evident in the annealed spectra. This feature completely dominates the spectra from samples annealed at higher temperatures. The feature present near 3.35 eV in the 700 ^{o}C anneal line was due to an extraneous light source in the lab, and is not from the sample.

The center of the band-edge feature is consistent with the expected donor bound exciton peak position for $Al_{0.1}Ga_{0.9}N$, leading to the conclusion that the Al mole fraction of 33% indicated by the grower was incorrect. The corrected value has been reported throughout this paper.[10:46] Another impurity emission peak appears at about 3.3 eV which can be attributed to donor-acceptor pair transitions. Judging magnetically, the strongest coercive field (best result) for this material was found at 750 ^{o}C but with very little variation above 700 ^{o}C.
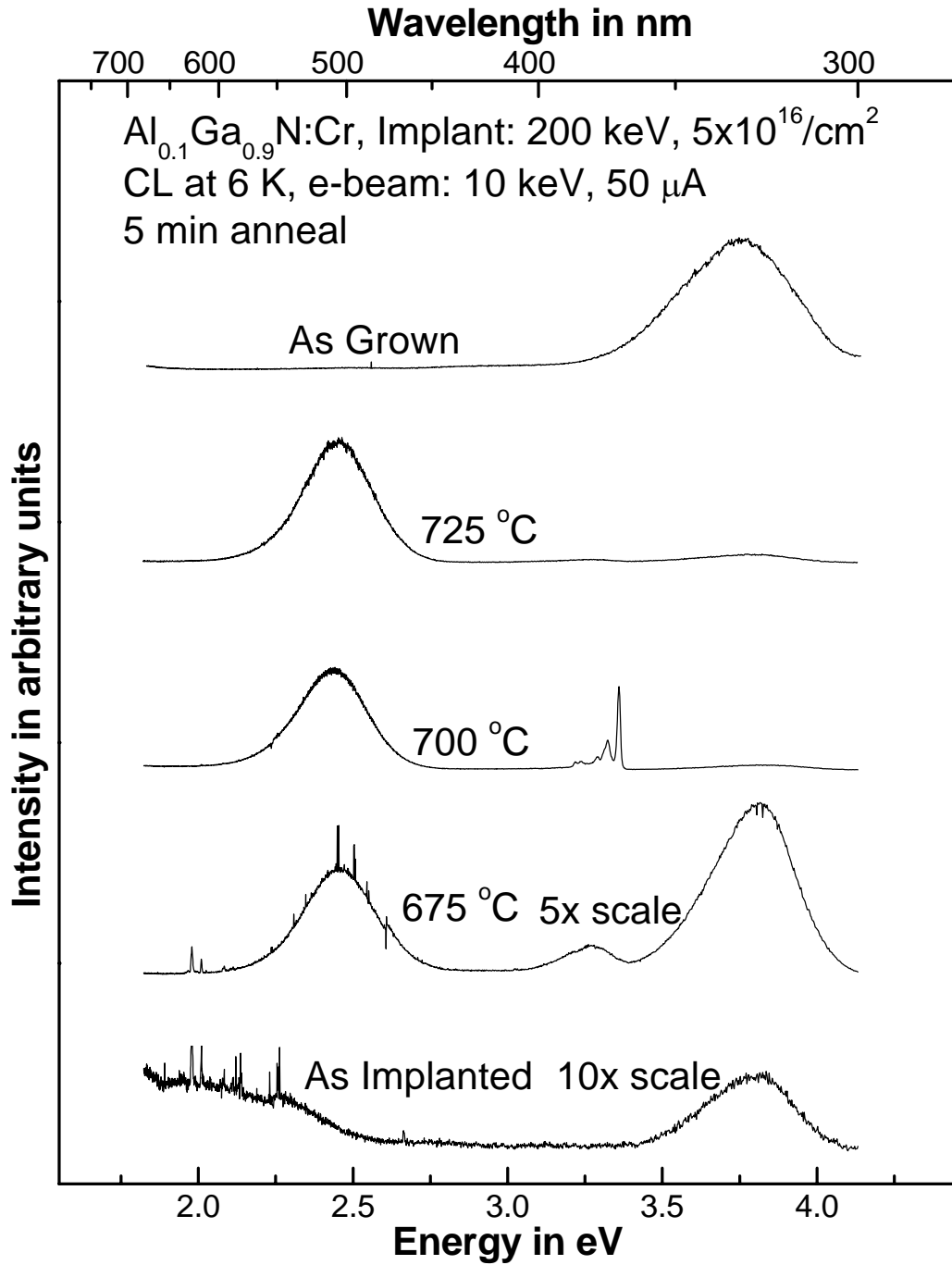
Figure 8. Cathodoluminescence spectra of $Al_{0.1}Ga_{0.9}N$:Cr as a function of annealing temperature. Spectra are shown from a 1 μm layer of $Al_{0.1}Ga_{0.9}N$ grown on a 2 μm AlN buffer layer, grown on sapphire, doped with chromium and annealed at the temperatures indicated.

Figure 9 shows CL results for $Al_{0.1}Ga_{0.9}N$ as-grown, as-implanted with Mn, and annealed at various temperatures. As before, the donor bound exciton peak appears near 3.75 eV consistent with $Al_{0.1}Ga_{0.9}N$, and the yellow luminescence is present in all but the as-grown case. Optically determined, the best anneal was at 675 ^{o}C for 5 min for this dopant with significant damage shown in higher temperature anneals by the increasing dominance of the yellow luminescence. Another impurity peak was present near 3.25 eV. The same anneal proved best magnetically as well, showing marked improvements over all higher anneal temperatures tested.

Figure 10 shows CL data for $Al_{0.1}Ga_{0.9}N$ as-grown, as-implanted with Ni, and annealed at various temperatures. The donor bound exciton peak was still consistent with $Al_{0.1}Ga_{0.9}N$ at around 3.75 eV. Once again, the optically determined best anneal was at 675 ^{o}C for 5 min, this time showing no yellow luminescence. In this case there was no apparent impurity emission in the range of the measurement and there were worse spectra for cases at both higher and lower anneal temperatures. The magnetically determined best anneal was 700 ^{o}C for 5 minutes, with worse measurements for both lower and higher anneal temperatures. This coercive field strength was comparable with that found with the optical best anneal case.

p-GaN

Figure 11 depicts CL spectra for p-GaN as-grown, as-implanted with Cr, and annealed at various temperatures. The band edge feature is near 3.6 eV which is at higher energy than that expected for an excitonic transition in GaN of just under 3.5 eV. This indicates the possibility that the luminescence is being detected from the AlN buffer
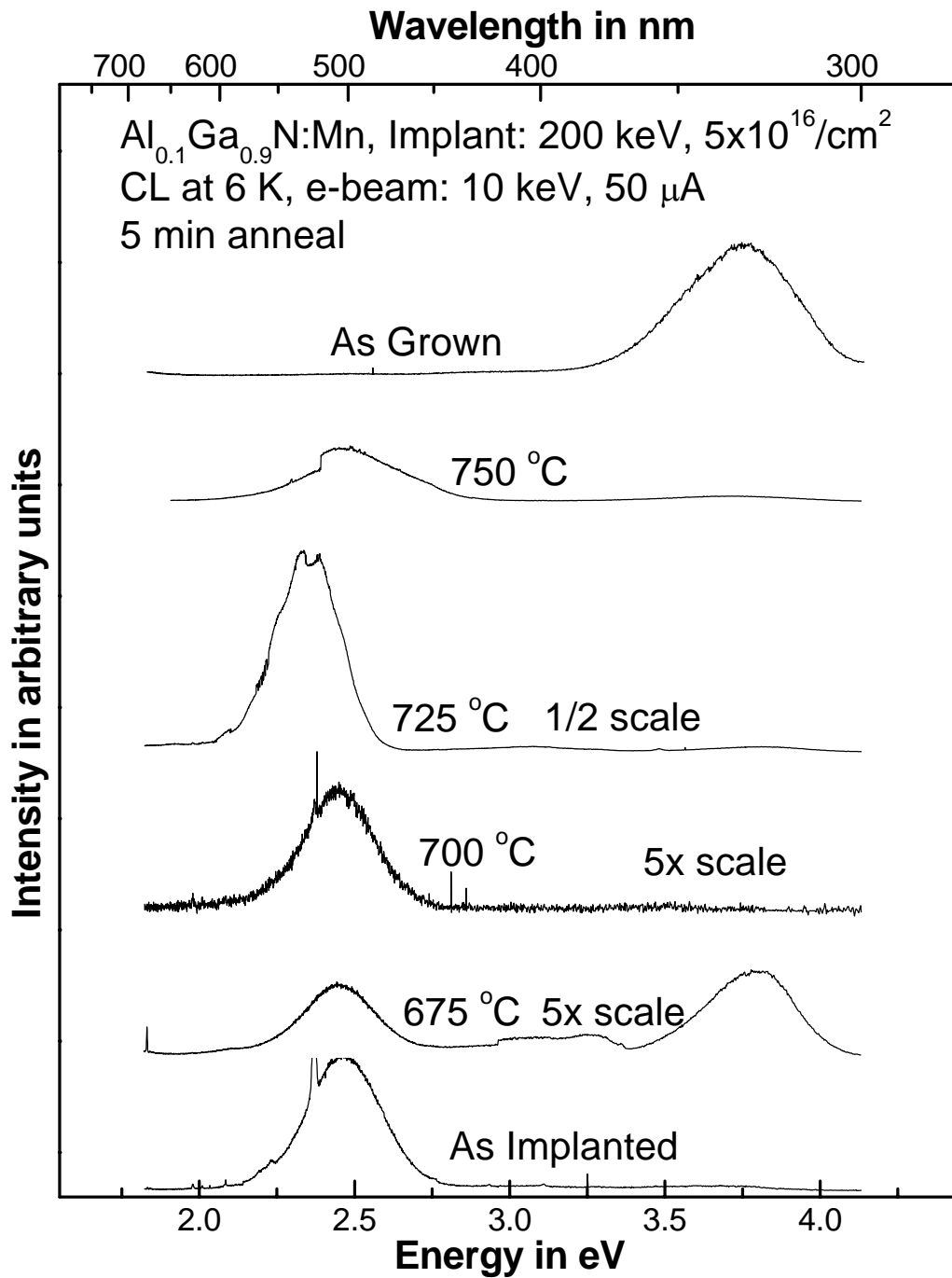
27

Figure 9. Cathodoluminescence spectra of $Al_{0.1}Ga_{0.9}N$:Mn as a function of annealing temperature. Spectra are shown from a 1 μm layer of $Al_{0.1}Ga_{0.9}N$ grown on a 2 μm AlN buffer layer, grown on sapphire, doped with manganese and annealed at the temperatures indicated.
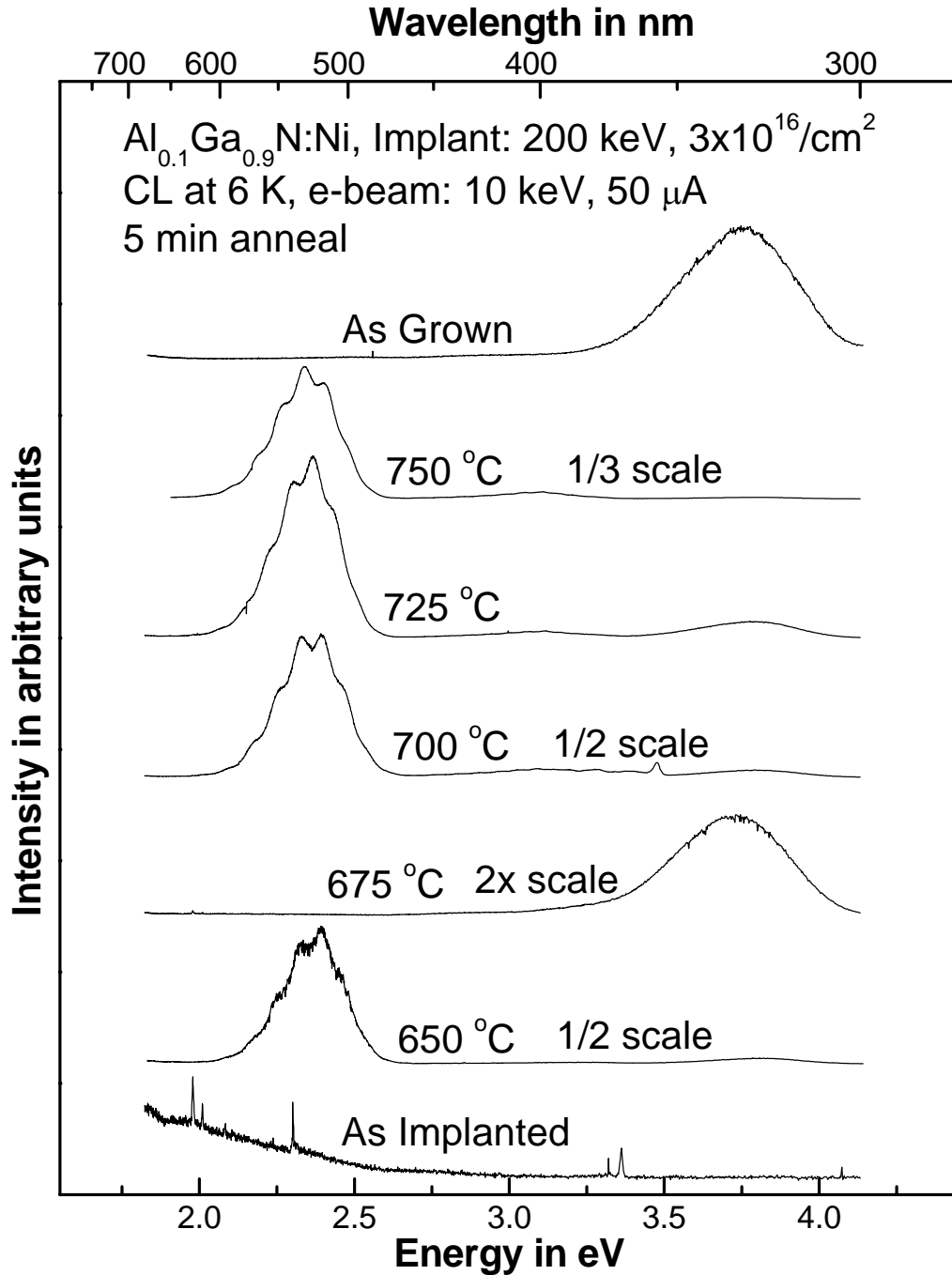
Figure 10. Cathodoluminescence spectra of $Al_{0.1}Ga_{0.9}N$:Ni as a function of annealing temperature. Spectra are shown from a 1 μm layer of $Al_{0.1}Ga_{0.9}N$ grown on a 2 μm AlN buffer layer, grown on sapphire, doped with nickel and annealed at the temperatures indicated.
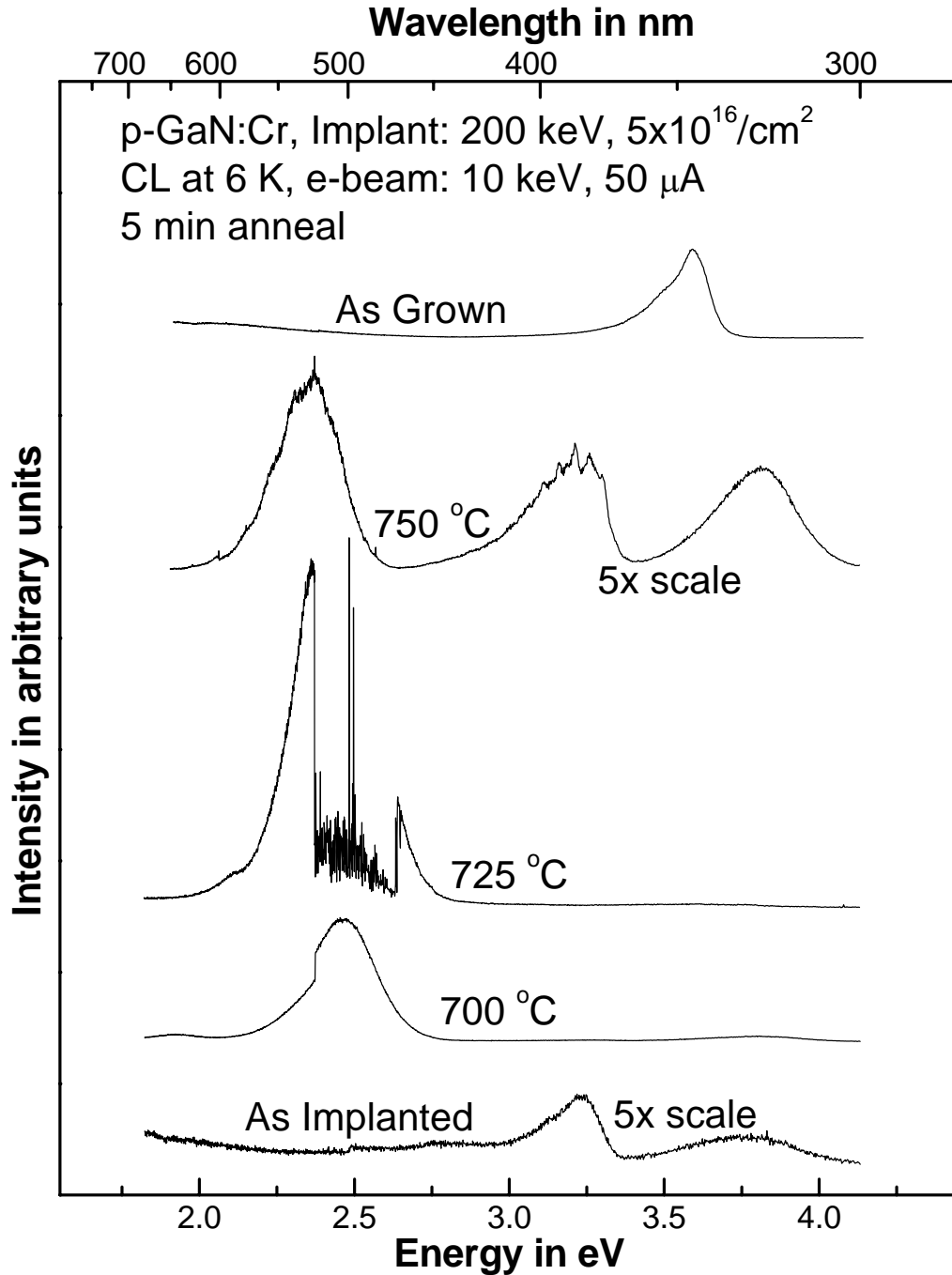
Figure 11. Cathodoluminescence spectra of p-GaN:Cr as a function of annealing temperature. Spectra are shown from a 1 μm layer of GaN:Mg (10^{17}/cm^3 Mg) grown on a 2 μm AlN buffer layer, grown on sapphire, doped with chromium and annealed at the temperatures indicated.

layer.[11]   Optically, the best anneal was 750 $^{\circ}$C for 5 min with significantly poorer results at lower temperatures. The poor quality of even this best case implies that the best annealing condition is likely at an even higher temperature. A prominent peak is present at 3.2 eV, but since this peak is also present in the as-implanted spectrum, it is probably not a valid impurity emission. Magnetically, the best case was an anneal of 725 $^{\circ}$C for 5 min, with weaker coercive fields at both lower and higher temperatures.

Figure 12 shows CL spectra for p-GaN as-grown, and annealed at various temperatures after implantation with Mn. The well-annealed samples clearly show a donor bound exciton peak at just below 3.5 eV as well as a donor acceptor pair peak near 3.25 eV with two optical phonon replicas.[11] This is a close fit to the expected values for GaN. Luminescence near 2.5 eV is also present these samples. It has been suggested that this is attributable to a donor-Mn acceptor pair transitions, and is not the typically observed yellow luminescence. [12]

The best anneal was at 675 $^{\circ}$C for 5 min as determined optically, with comparable results when annealed at 750 $^{\circ}$C, and worse results at anneal temperatures between these values. Magnetically, the best anneal was 725 $^{\circ}$C for 5 min, with significantly weaker coercive fields at lower anneal temperatures and comparable results when annealed at 750 $^{\circ}$C.

Figure 13 shows CL spectra for p-GaN as-grown, as-implanted with Ni, and annealed at various temperatures. Once again higher than expected energies were found as a band gap feature. Optically, the best anneal was found at 675 $^{\circ}$C for 5 min, with worse results at both higher and lower anneal temperatures. A donor acceptor pair peak
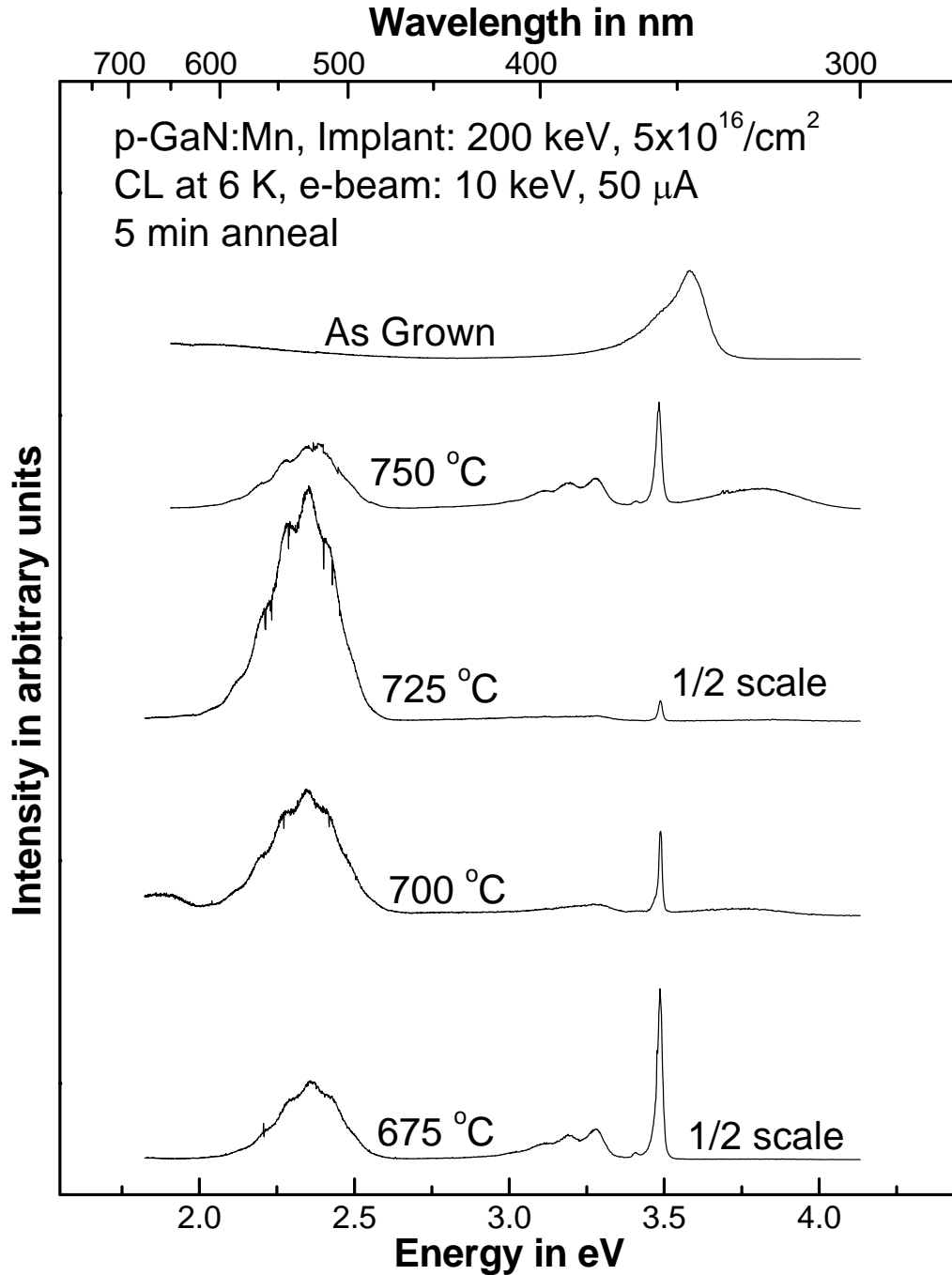
31

Figure 12. Cathodoluminescence spectra of p-GaN:Mn as a function of annealing temperature. Spectra are shown from a 1 μm layer of GaN:Mg (10^{17}/cm^3 Mg) grown on a 2 μm AlN buffer layer, grown on sapphire, doped with manganese and annealed at the temperatures indicated.
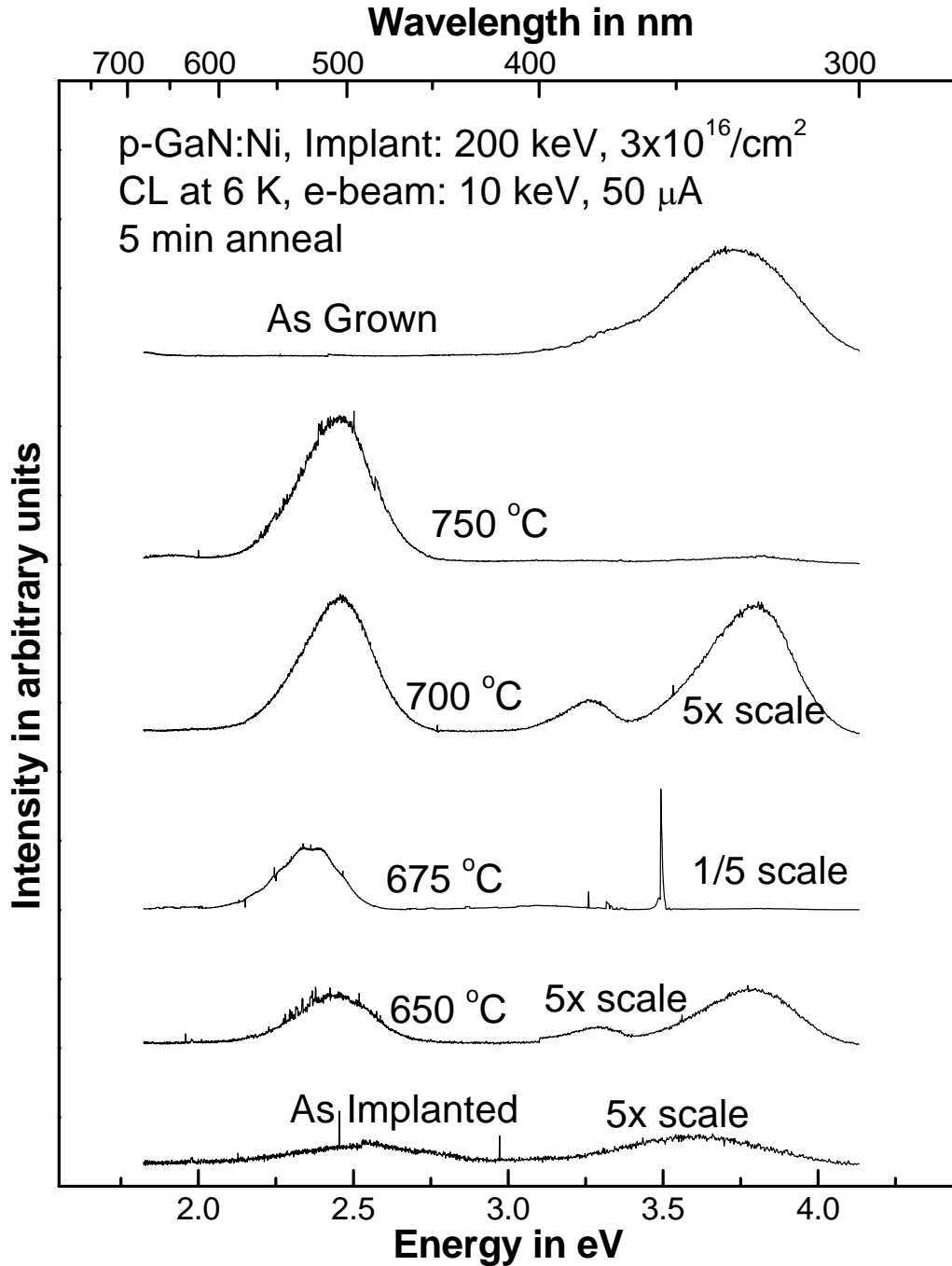
Figure 13. Cathodoluminescence spectra of p-GaN:Ni as a function of annealing temperature. Spectra are shown from a 1 µm layer of GaN:Mg (10^{17}/cm^3 Mg) grown on a 2 µm AlN buffer layer, grown on sapphire, doped with nickel and annealed at the temperatures indicated.

was noted at 3.25 eV. Magnetically, 675 ^{o}C for 5 minutes was by far the best anneal, also with worse results on both anneal temperature extremes.

ZnO

Figure 14 shows CL spectra for ZnO as-grown, as-implanted with Cr, and annealed at various temperatures. The band edge feature near 3.3 eV is attributed to bound exciton transitions, this may also be the merging of donor and acceptor bound exciton peaks.[13] Optically, the best anneal was 700 ^{o}C for 10 min. Other than intensity of the band edge feature, there is no significant change in the quality of the anneal at any anneal temperature over 650 ^{o}C. Magnetically, the best case was the anneal of 725 ^{o}C for 10 min, with lower coercive field strengths at both lower and higher anneal temperatures, but comparable measurements when annealed at any temperature from 675 to 725 ^{o}C.

Figure 15 shows CL spectra for ZnO as-grown, as-implanted with Mn, and annealed at various temperatures. The same exciton peak observed in ZnO:Cr is present near 3.3 eV. The best anneal for optical properties was at 675 ^{o}C for 10 min, with comparable results at all anneal temperatures from 675 to 725 ^{o}C. Magnetically, the best anneal was 700 ^{o}C for 10 min, with weaker coercive fields at both lower and higher anneal temperatures, but comparable measurements when annealed from 675 to 725 ^{o}C.

Figure 16 displays CL spectra for ZnO as-grown, as-implanted with Ni, and annealed at various temperatures. Once again, the exciton peak is apparent at 3.3 eV. From the spectra, the best anneal was 650 ^{o}C for 10 min. A broad emission near 2.55 eV was observed that may be the documented green luminescence common to ZnO. Since
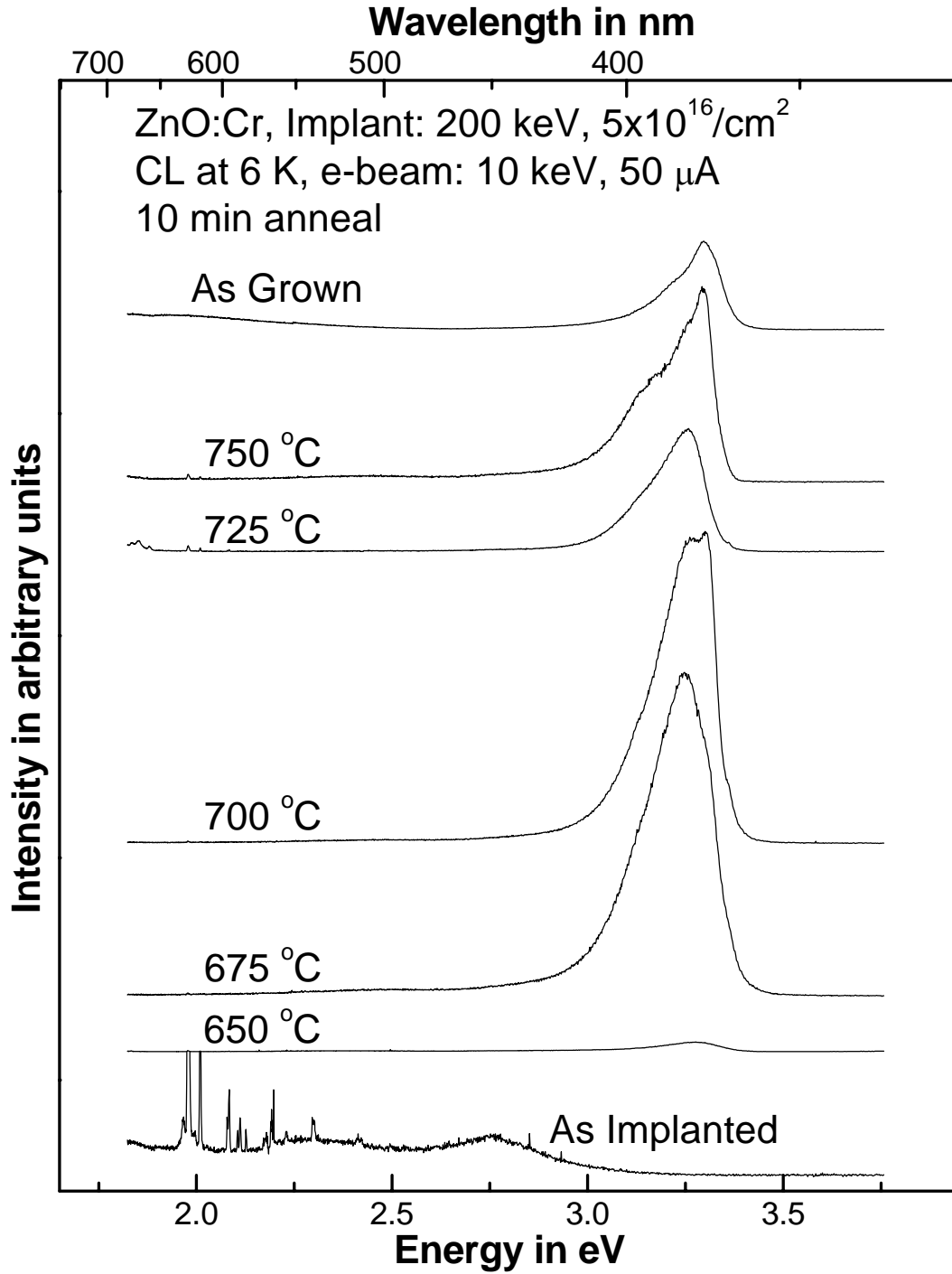
34

Figure 14. Cathodoluminescence spectra of ZnO:Cr as a function of annealing
temperature. Spectra are shown from a 1 μm layer of ZnO grown on
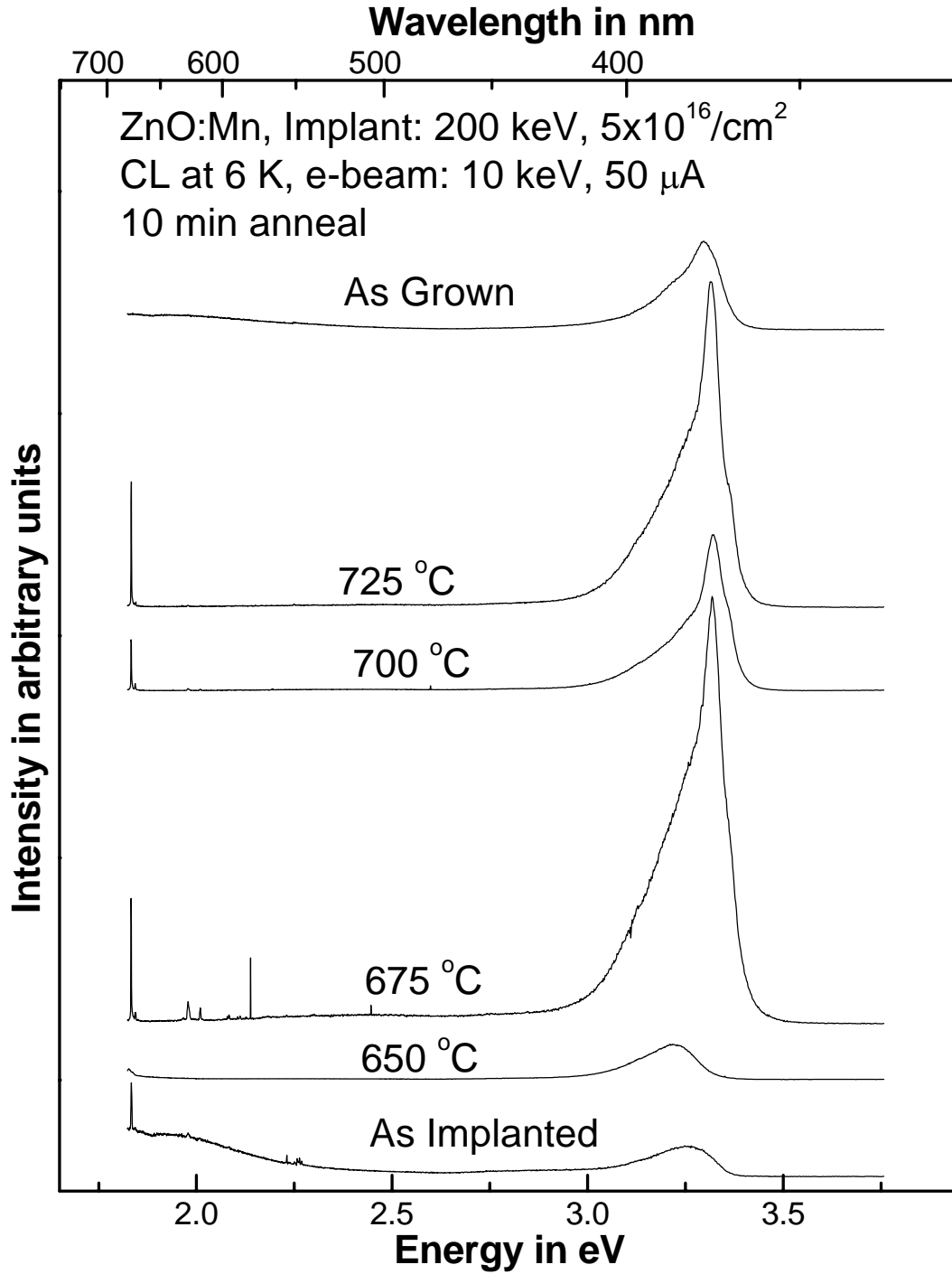sapphire, doped with chromium and annealed at the temperatures
indicated.

Figure 15. Cathodoluminescence spectra of ZnO:Mn as a function of annealing temperature. Spectra are shown from a 1 μm layer of ZnO grown on sapphire, doped with manganese and annealed at the temperatures indicated.
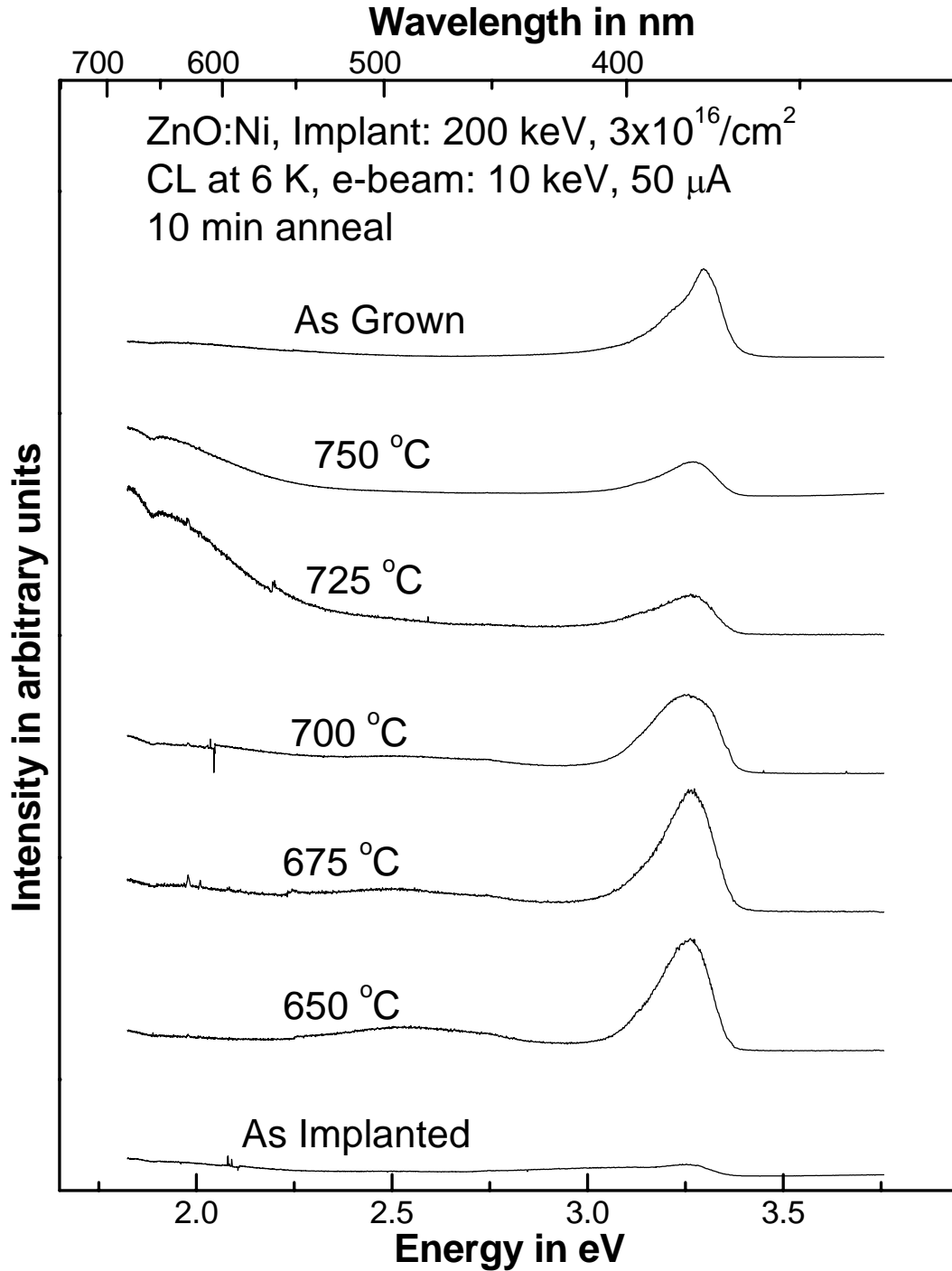
Figure 16. Cathodoluminescence spectra of ZnO:Ni as a function of annealing temperature. Spectra are shown from a 1 μm layer of ZnO grown on sapphire, doped with nickel and annealed at the temperatures indicated.

this feature has not been common to these samples, it is possible that it is actually an impurity-related peak.   For magnetic properties, 725 $^{\circ}$C for 10 min was the best anneal with comparable results when annealed at 675 $^{\circ}$C and significantly weaker coercive fields when annealed at higher temperatures.

Summary

This chapter has presented the results obtained in taking measurements for this project. It has interpreted these results for each material/dopant combination according to both optical and magnetic criteria. The following chapter will provide an overview of what was accomplished in this project, as well as present a more concise description of the most significant results observed. Finally, it will point out future related work, and discuss the progress made.

V. Conclusions and Recommendations

This primary objective of this research was to investigate the effects of annealing temperatures on the optical and magnetic properties of transition-metal doped wide band gap semiconductors. For this purpose 1 µm thick films of $Al_{0.1}Ga_{0.9}N$, magnesium doped p-GaN, and ZnO grown on sapphire were implanted at 200 keV with 5×10^{16} cm^{-2} chromium or manganese, or 3×10^{16} cm^{-2} nickel, and investigated both optically by cathodoluminescence, and magnetically by superconducting quantum interference device (SQuID) measurements. The goal was to work toward developing room temperature dilute magnetic semiconductors.

Optimal annealing temperatures were determined separately for optical and magnetic purposes to within 25 ^{o}C for each material combination, with trends noted, and material properties reported as applicable.

The results of cathodoluminescence measurements demonstrated a pattern by which transitions near the band edge dominate the spectra in as-grown samples, then are in turn dominated by other emissions after implantation. These band edge features are gradually returned to prominence in the annealed samples, reaching a maximum in the best annealed cases, and finally reduced in prominence in cases of over-annealing.

The cathodoluminescence spectra show that for $Al_{0.1}Ga_{0.9}N$, a possible magnetic impurity related peak appears near 3.3 eV when implanted with Cr, and near 3.25 eV when implanted with Mn. These results also show an apparent magnetic impurity related peak in ZnO near 2.55 eV when implanted with Ni.

Manganese-implanted $Al_{0.1}Ga_{0.9}N$ annealed at 675 ^{o}C and nickel implanted p-GaN annealed at 675 ^{o}C both demonstrated the best crystal recovery and optimum

39

magnetic response under the same annealing conditions. For this reason they are the most promising combinations of materials and annealing recipes tested.

Also of major interest were those combinations which, while not showing a perfect match with the same anneal giving the optimum results by both measures, exhibit an annealing case or cases with favorable results in both tests. However, chromium implanted $Al_{0.1}Ga_{0.9}N$ and chromium implanted p-GaN showed no overlap between favorable results by these two measurements.

All of these material combinations showed at least one annealing recipe that provided good hysteresis results, and at least one case with a promising optical anneal. They may all be useful in one field or the other, only for applications that need both qualities should investigations be limited to the more promising materials as presented here.

There are several suggestions for continuing research efforts in this area. First, this study was limited in its range of temperatures investigated. Further work could be done by extending the limits of the study for all materials in which the best anneal was found to be at 650 ^{o}C on the low end, and 750 ^{o}C on the high end. Further investigation could also refine these results by narrowing the temperature increments, and by exploring longer anneal times for all cases.

For materials found to be promising both magnetically and optically, there is much more work to be done. The materials would need to be tested at room temperature both optically and magnetically, to ensure that the observed behavior will lend itself to a useable device. Another significant step in this research is to investigate the effect, if any of a stored field on the optical response of the material. Specifically, it is suspected that there may be a useable broadening of impurity emissions with a stored field.
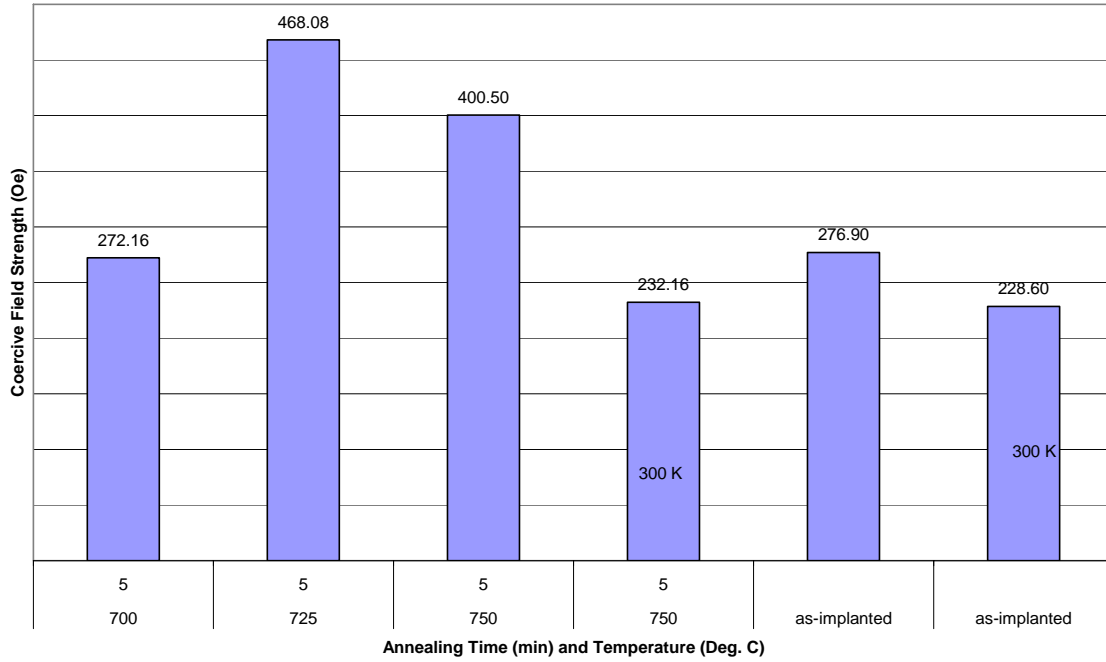
40

Progress was made during this project toward the development of room temperature dilute magnetic semiconductors. Material combinations were evaluated for suitability for this type of work. Annealing temperatures were investigated, providing guidance for future researchers to begin their work in this area. Finally, the knowledge base for wide band gap semiconductors was increased, allowing an incremental step toward bringing wide band gap semiconductor development to a par with traditional semiconductor technology.

41

Appendix: Preliminary Hysteresis Measurement Results

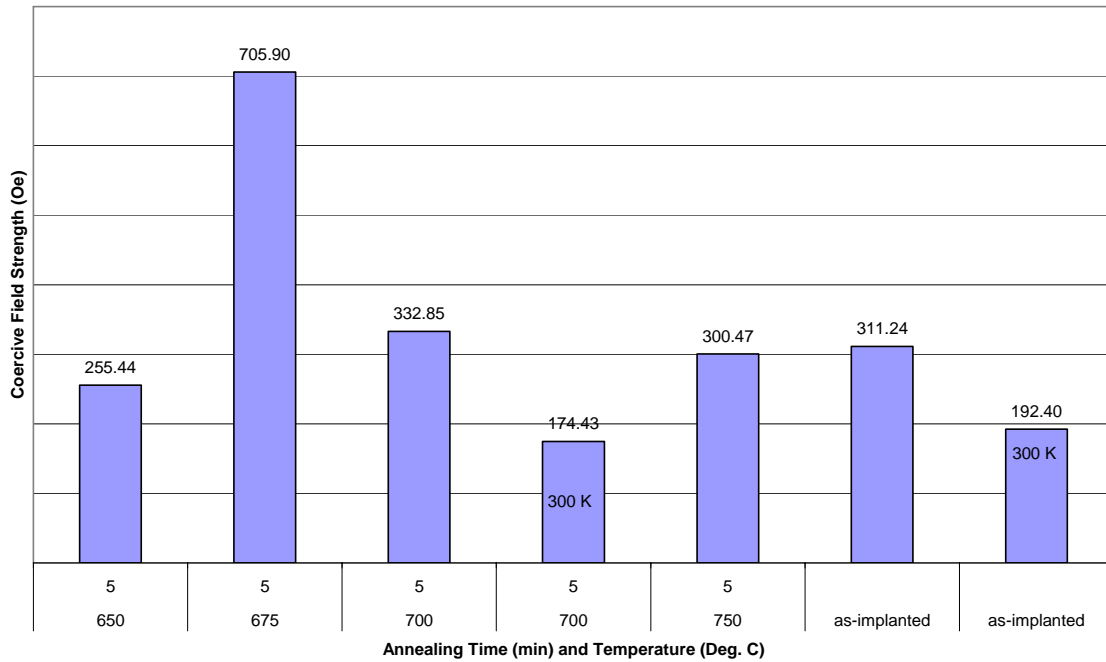Charts of coercive field strength of each material at each annealing condition:
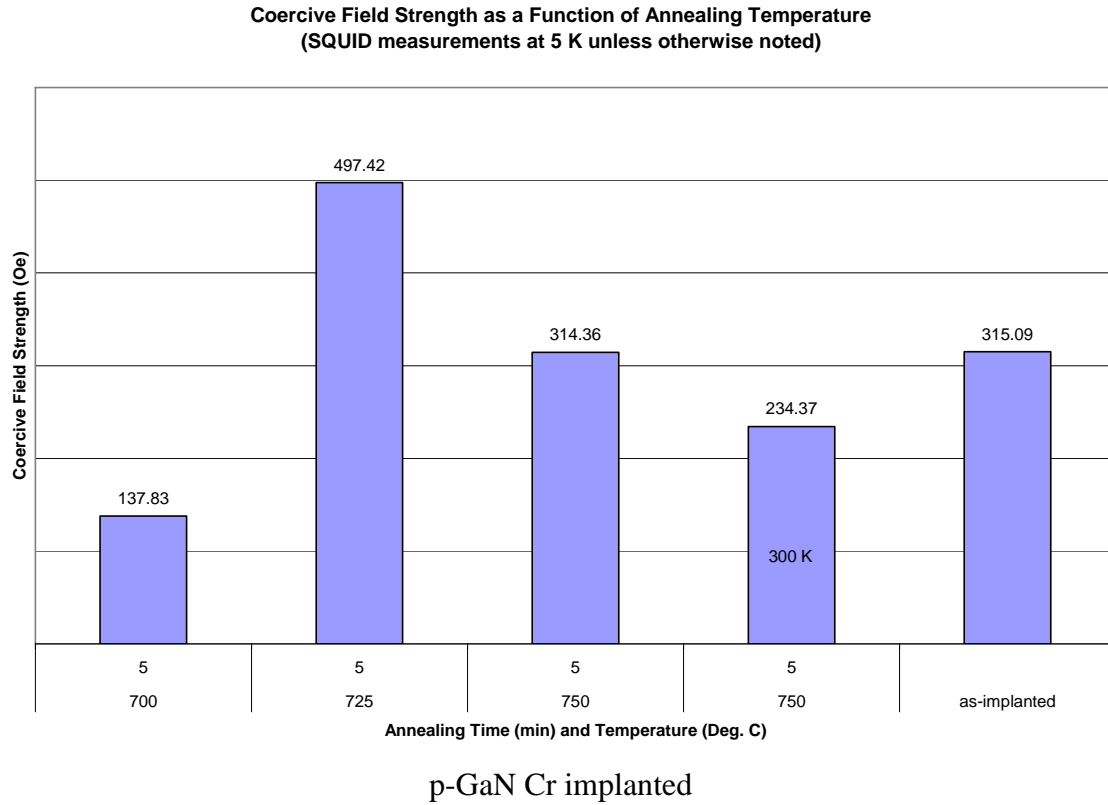
Coercive Field Strength as a Function of Annealing Temperature
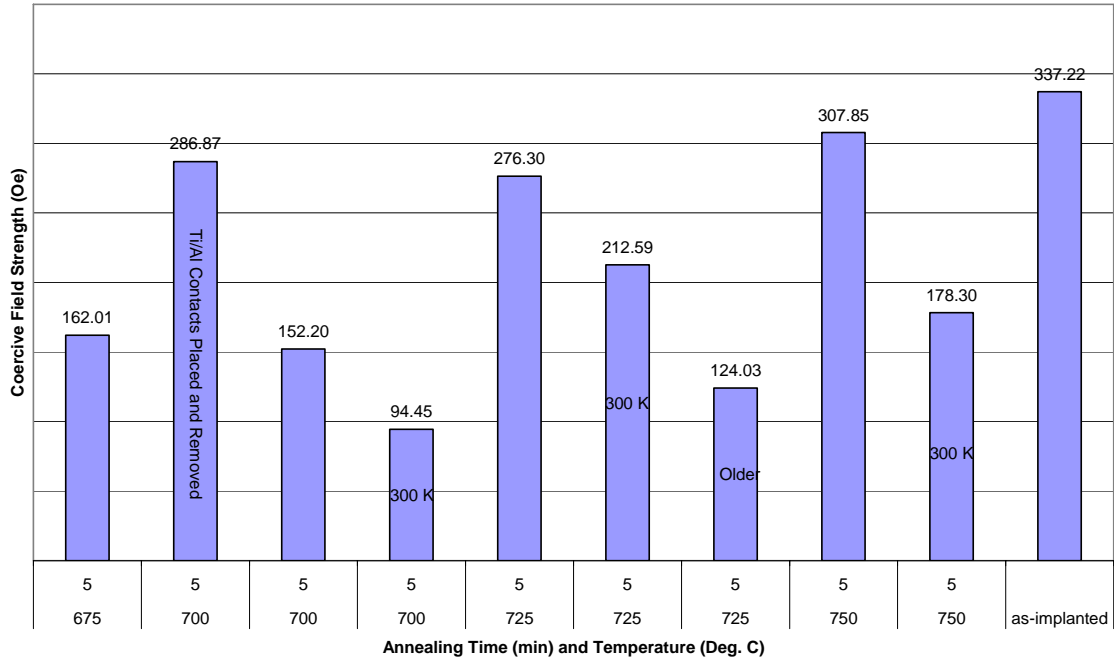**(SQUID measurements at 5 K unless otherwise noted)**

	5	5	5	5	as-implanted
	700	725	750	750	

Bar values: 137.83, 497.42, 314.36, 234.37 (300 K), 315.09

Y-axis: Coercive Field Strength (Oe)
X-axis: Annealing Time (min) and Temperature (Deg. C)

p-GaN Cr implanted

Coercive Field Strength as a Function of Annealing Temperature
(SQUID measurements at 5 K unless otherwise noted)

272.16	468.08	400.50	232.16 (300 K)	276.90	228.60 (300 K)
5	5	5	5	as-implanted	as-implanted
700	725	750	750		

Annealing Time (min) and Temperature (Deg. C)

p-GaN Mn implanted

Coercive Field Strength as a Function of Annealing Temperature
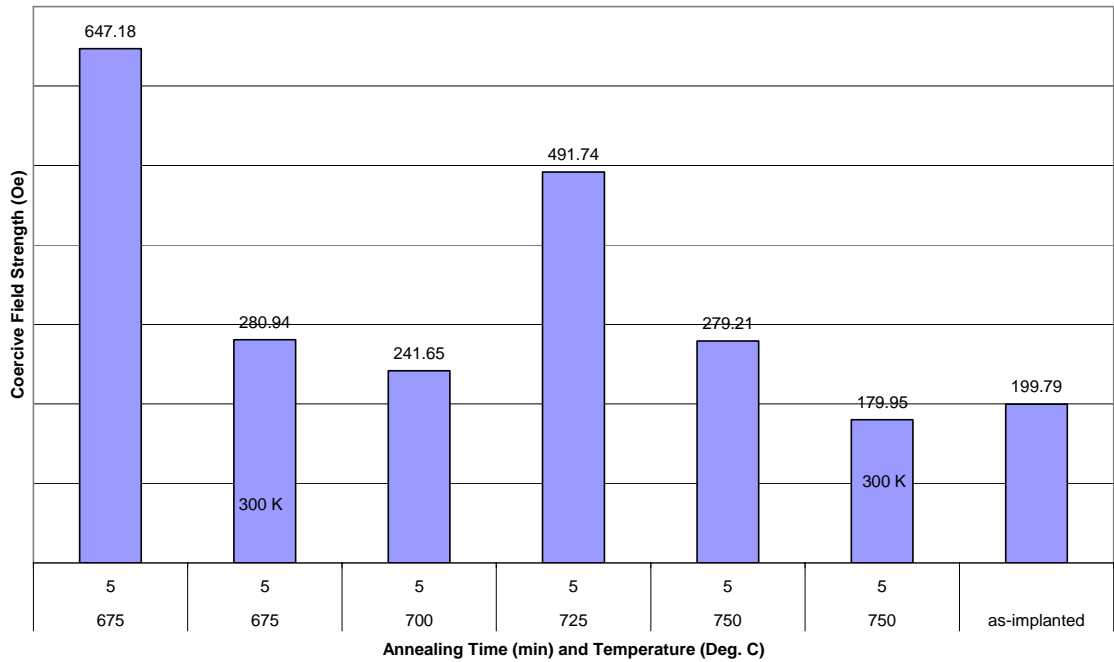**(SQUID measurements at 5 K unless otherwise noted)**

255.44	705.90	332.85	174.43 (300 K)	300.47	311.24	192.40 (300 K)
5	5	5	5	5	as-implanted	as-implanted
650	675	700	700	750		

Annealing Time (min) and Temperature (Deg. C)

p-GaN Ni implanted

43

Coercive Field Strength as a Function of Annealing Temperature
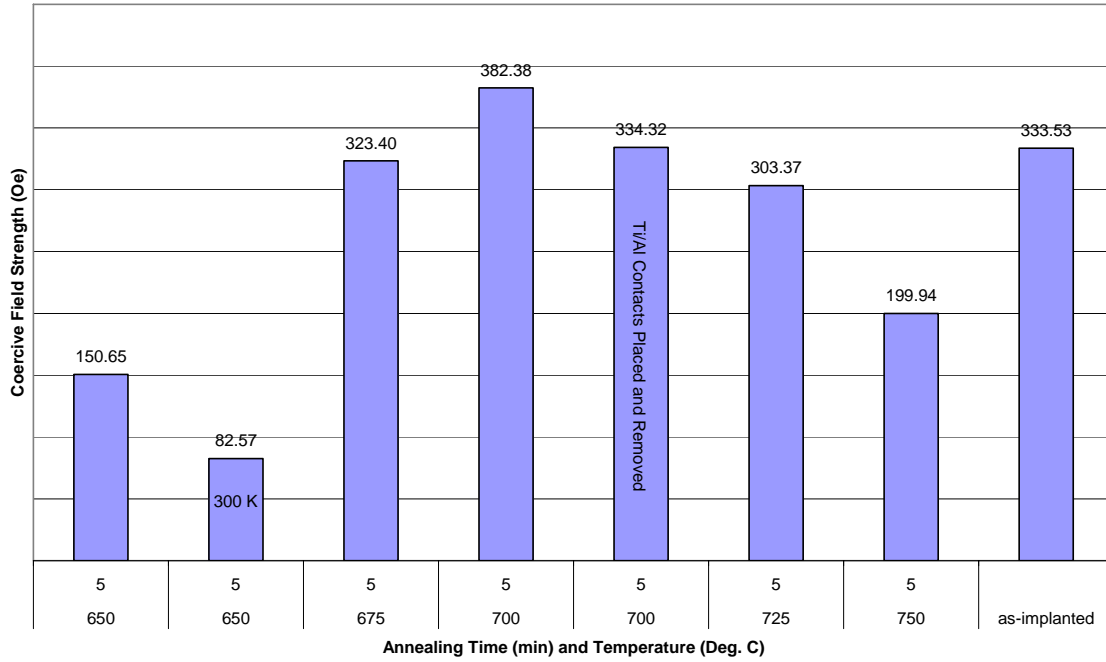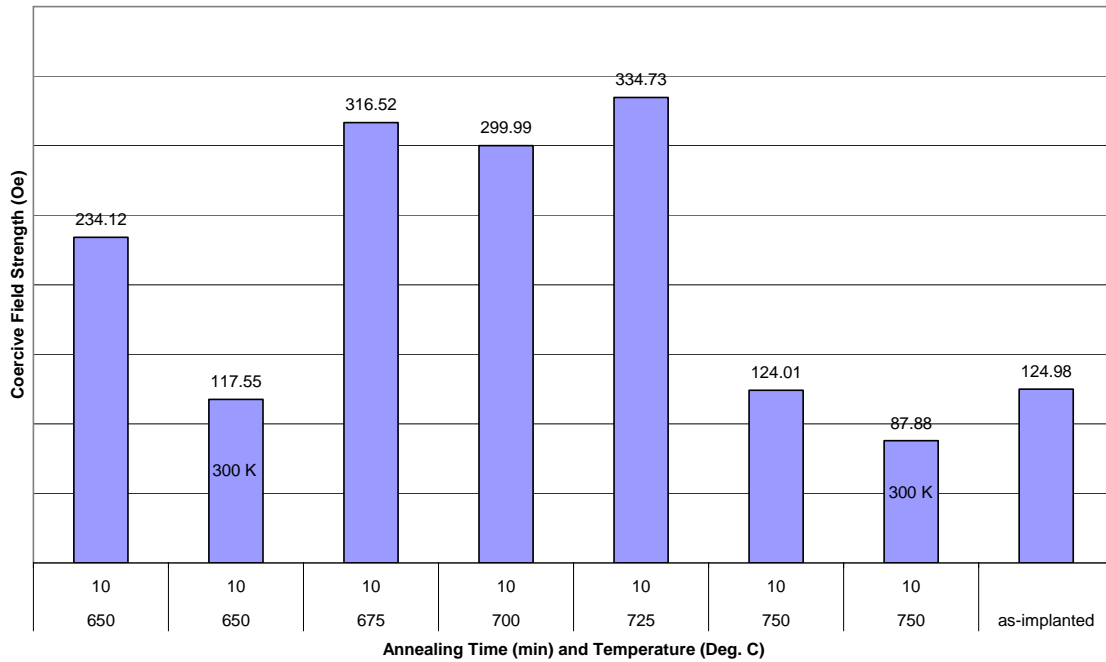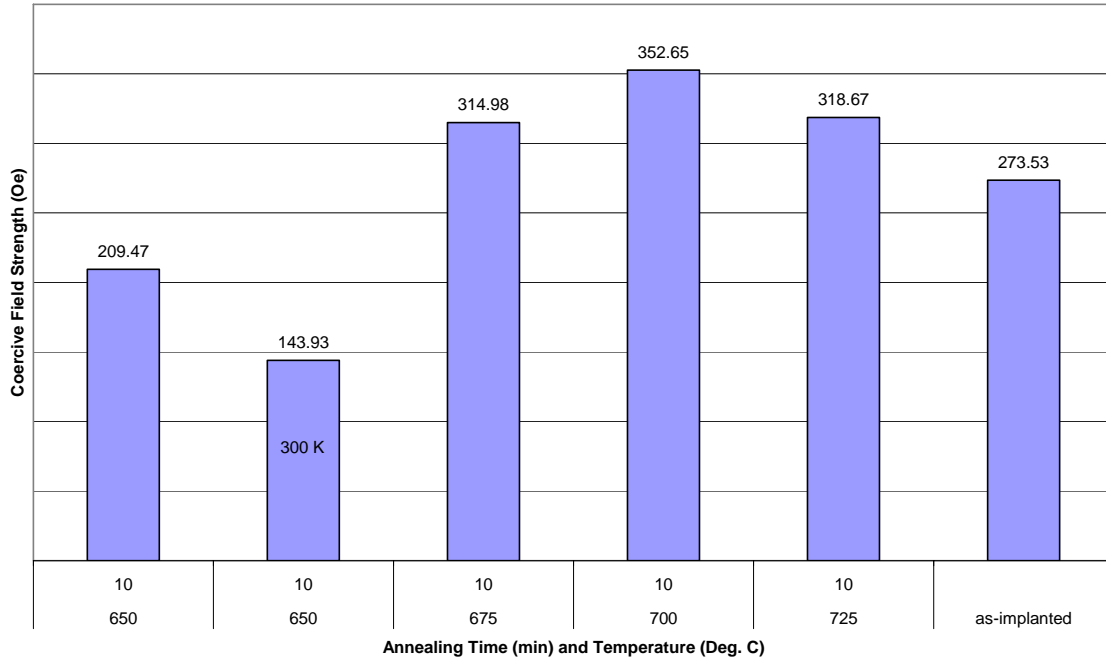**(SQUID measurements at 5 K unless otherwise noted)**

$Al_{0.1}Ga_{0.9}N$ Cr implanted

Coercive Field Strength as a Function of Annealing Temperature
(SQUID measurements at 5 K unless otherwise noted)

$Al_{0.1}Ga_{0.9}N$ Mn implanted

44

Coercive Field Strength as a Function of Annealing Temperature
(SQUID measurements at 5 K unless otherwise noted)

$Al_{0.1}Ga_{0.9}N$ Ni implanted

Coercive Field Strength as a Function of Annealing Temperature
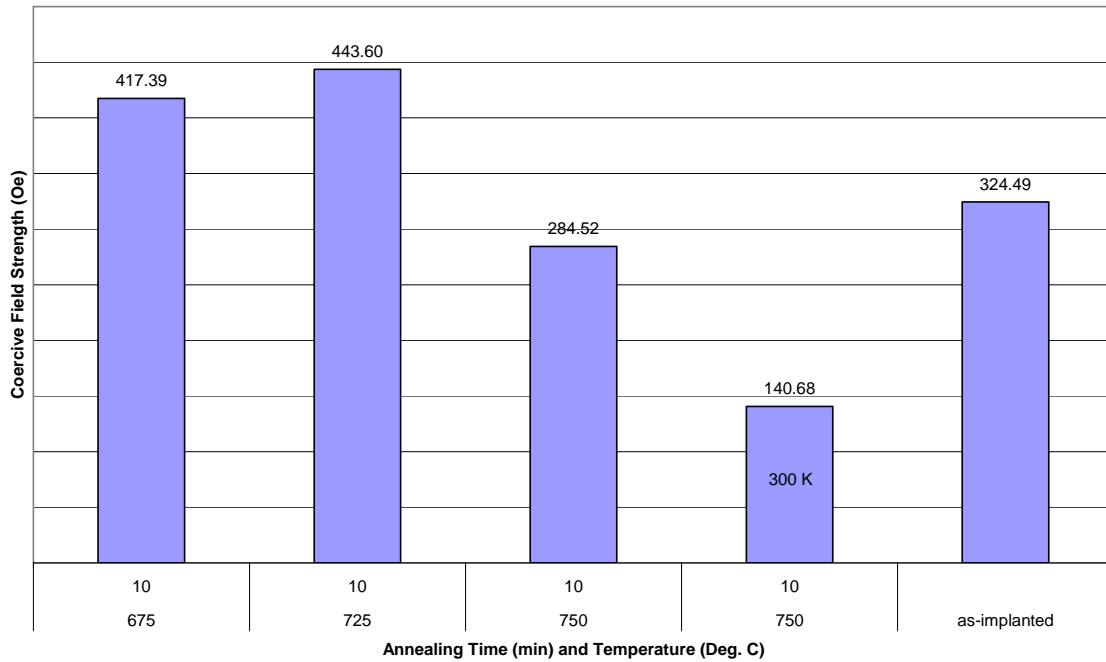**(SQUID measurements at 5 K unless otherwise noted)**

ZnO Cr implanted

45

Coercive Field Strength as a Function of Annealing Temperature
(SQUID measurements at 5 K unless otherwise noted)

ZnO Mn implanted

Coercive Field Strength as a Function of Annealing Temperature
(SQUID measurements at 5 K unless otherwise noted)

ZnO Ni implanted

46

Bibliography

1. McKelvey, John P., *Solid State Physics*. FL: Krieger Publishing Company, 1993.

2. Sze, S. M., *Semiconductor Devices Physics and Technology Second Edition*. New York: John Wiley and Sons, 2002.

3. Polyakov, A. Y., Govorkov, A. V., Smirnov. N. B., Pashkova, N. Y., Thaler, G. T., Overberg, M. E., Frazier, R., Abernathy, C. R., Pearton, S. J., Kim, Jihyun, and Ren, F. *Optical and electrical properties of GaMnN films grown by molecular beam epitaxy.* Journal of Applied Physics Volume 92, Number 9. 30 July 2002.

4. Structured Material Industries Inc., *Featured Material: Zn(Mg)O*. www.structuredmaterials.com downloaded 1 Jan 2005.

5. Bhattacharya, Pallab., *Semiconductor Optoelectronic Devices Second Edition*. NJ: Prentice Hall, 1997.

6. Colton, John Snyder. *Selective Excitation of the Yellow and Blue Luminescence in n- and p-implanted Gallium Nitride*. Doctoral Dissertation, University of California, Berkeley, CA: Fall 2000.

7. Reynolds, D. C., Look, D. C., Jogai, B., and Morkoc, H. *Similarities in the Bandedge and Deep-Centre Photoluminescence Mechanisms of ZnO and GaN*. Solid State Communications Volume 101 Number 9. Great Britain: Elsevier Science Ltd, 1997.

8. Yeo, Yung Kee. *Request for Peer Safety Review and Self-Study Documentation*. Wright-Patterson AFB, OH: Department of Engineering Physics, Air Force Institute of Technology (AU), 11 February 2004.

9. University of Ottowa. Astronomy Knowledge Base http://www.csi.uottowa.ca:4321/astronomy/ Canada: downloaded 11 November 2004.

10. McFall, J. L. Hengehold, R.L. and Yeo, Yung Kee. *Optical Investigation of MBE Grown Si-Doped $Al_xGa_{1-x}N$ as a Function of Nominal Al Mole Fraction up to 0.5*. Wright-Patterson AFB, OH: Air Force Institute of Technology (AU).

11. Fellows, James A., Yeo, Yung Kee, Ryu, Mee-Yi and Hengehold, R. L. *Optical study of implantation damage recovery from Si-implanted GaN*. Wright-Patterson AFB, OH: Air Force Institute of Technology (AU), 4 November 2004.

12. Shon, Yoon, Kwon, Young Hae, Yuldashev, Sh. U., Leem, J. H., Park, C. S., Fu, D. J., Kim, H. J. and Kang, T. W. *Optical and magnetic measurements of p-type GaN epilayers implanted with Mn$^+$ ions.* Applied Physics Letters Volume 81, Number 10. 22 July 2002.

13. Sun, X. W. and Kwok, H. S. *Optical properties of epitaxially grown zinc oxide films on sapphire by pulsed laser deposition.* Journal of Applied Physics Volume 86, Number 1. 1 July 1999.

1. REPORT DATE (DD-MM-YYYY) 21-03-2005	2. REPORT TYPE Master's Thesis	3. DATES COVERED (From – To) Aug 2003 – Mar 2005

4. TITLE AND SUBTITLE	5a. CONTRACT NUMBER
OPTICAL INVESTIGATION OF TRANSITION METAL IMPLANTED WIDE BAND GAP SEMICONDUCTORS	5b. GRANT NUMBER
	5c. PROGRAM ELEMENT NUMBER
6. AUTHOR(S) Feller, Brian, P., First Lieutenant, USAF	5d. PROJECT NUMBER
	5e. TASK NUMBER
	5f. WORK UNIT NUMBER

7. PERFORMING ORGANIZATION NAMES(S) AND ADDRESS(S) Air Force Institute of Technology Graduate School of Engineering and Management (AFIT/EN) 2950 Hobson Way WPAFB OH 45433-7765	8. PERFORMING ORGANIZATION REPORT NUMBER AFIT/GEO/ENP/05-02

9. SPONSORING/MONITORING AGENCY NAME(S) AND ADDRESS(ES) N/A	10. SPONSOR/MONITOR'S ACRONYM(S)
	11. SPONSOR/MONITOR'S REPORT NUMBER(S)

12. DISTRIBUTION/AVAILABILITY STATEMENT
APPROVED FOR PUBLIC RELEASE; DISTRIBUTION UNLIMITED

13. SUPPLEMENTARY NOTES

Thin films of GaN, $Al_{0.1}Ga_{0.9}N$, and ZnO were implanted with Cr, Mn, and nickel Ni to produce dilute magnetic semiconductors. Optical and magnetic techniques were used to evaluate crystal structure restoration and coercive field strength as a function of implant species and annealing temperature. Maximum crystal restoration was obtained for $Al_{0.1}Ga_{0.9}N$ after annealing at 675 ^{o}C; for Cr implanted p-GaN after annealing at 750 ^{o}C; for Mn or Ni implanted p-GaN after annealing at 675 ^{o}C; for Cr implanted ZnO after annealing at 700 ^{o}C; for Mn implanted ZnO after annealing at 675 ^{o}C; and for Ni implanted ZnO after annealing at 650 ^{o}C. Maximum coercive field strengths were found for Cr implanted $Al_{0.1}Ga_{0.9}N$ after annealing at 750 ^{o}C; for Mn implanted $Al_{0.1}Ga_{0.9}N$ after annealing at 675 ^{o}C; for Ni implanted $Al_{0.1}Ga_{0.9}N$ after annealing at 700 ^{o}C; for Cr or Mn implanted p-GaN after annealing at 725 ^{o}C; for Ni implanted p-GaN after annealing at 675 ^{o}C; for Cr or Ni implanted ZnO after annealing at 725 ^{o}C; and for Mn implanted ZnO after annealing at 725 ^{o}C. Optimum annealing conditions for optical and magnetic properties of the implanted wide band gap semiconductors agree with each other very well.

15. SUBJECT TERMS
Wide Gap Semiconductors, Annealing, ZnO, GaN, AlGaN, Ferromagnetic Materials, Optical Properties, Magnetic Properties

16. SECURITY CLASSIFICATION OF:			17. LIMITATION OF ABSTRACT	18. NUMBER OF PAGES	19a. NAME OF RESPONSIBLE PERSON Yung Kee Yeo
REPORT U	ABSTRACT U	c. THIS PAGE U	UU	60	19b. TELEPHONE NUMBER (Include area code) (937) 785-3636 x4532

Standard Form 298 (Rev: 8-98)
Prescribed by ANSI Std. Z39-18